Coastal Engineering 157 (2020) 103656

Contents lists available at ScienceDirect

Coastal Engineering

journal homepage: http://www.elsevier.com/locate/coastaleng

Large-scale hurricane modeling using domain decomposition parallelization and implicit scheme implemented in WAVEWATCH III wave model

Ali Abdolali [a,b,*], Aron Roland [c], Andre van der Westhuysen [a,b], Jessica Meixner [a], Arun Chawla [a], Tyler J. Hesser [d], Jane M. Smith [d], Mathieu Dutour Sikiric [e]

[a] NWS/NCEP/Environmental Modeling Center, National Oceanic and Atmospheric Administration (NOAA), College Park, MD, USA
[b] I.M. Systems Group, Inc. (IMSG), Rockville, MD, 20852, USA
[c] BGS IT & E, Darmstadt, Hesse, Germany
[d] US Army Engineer Research and Development Center, Coastal and Hydraulics Laboratory, Vicksburg, MS, USA
[e] Laboratory for Physic of the Sea and Chemistry of Water Systems, Rudjer Bošković Institute, Zagreb, Croatia

ARTICLE INFO

Keywords:
Parallelization
Domain decomposition
Implicit solver
Spectral wave model
WAVEWATCH III

ABSTRACT

WAVEWATCH III has been equipped with a new parallelization algorithm, domain decomposition and an optional implicit numerical scheme for coastal application at high spatial resolution with triangular unstructured grids, compatible with community-based coupling infrastructure. We performed a validation study for Hurricane Ike (2008) to prove the accuracy of the updated model against satellite altimeter data and buoy observations on various grids, forced by two sophisticated atmospheric models for hurricane simulation, using different solution schemes and parallelization algorithms. The new implementations for triangular grids are computationally efficient and scalable to be run on a large number of computational nodes, which constitutes a major breakthrough in the context of increasing needs for high-resolution nearshore wave modeling, making WAVEWATCH III (WW3) a powerful tool to simulate the sea state in the nearshore at high resolution and study wave-surge interactions in inner shelf regions.

1. Introduction

WW3 is a major spectral wave modeling system known for its applicability in large-scale modeling of sea states and wave climate from large rectilinear grids offshore to high-resolution unstructured grids in coastal zones (WW3DG, 2019). WW3 is widely applied in operational, research and engineering arenas. The model was initially designed for a global regular grid and later was extended to the multi-grid, the Spherical Multiple-Cell (SMC) and unstructured triangular grids for applications in nearshore waters. With the multi-grid capabilities, various rectilinear grids are nested internally to represent the offshore domain with a less computationally expensive coarse grid while the nearshore is run at a high-resolution (Tolman, 2008). The unstructured SMC grid was implemented in the WW3 model to overcome the polar problems, achieve enough resolution near the coast and improve computational time (Li, 2012). Introducing the unstructured triangular grids in the model avoid the complications in the multi-grid at the same time resolving complex shorelines. Studies have shown improvement in the accuracy of the model due to better representation of geometrical features (i.e., shoreline), forcing conditions and physics parameterization. As the grid resolution becomes finer, more sophisticated numerical schemes than CFL dependent explicit solvers which are governed by the minimum grid size are required. Thus, the unstructured grids require optimization to avoid computational slow down with an explicit solver or a robust numerical solver (i.e., implicit) to handle small grid elements. In addition and due to the increase demands for larger grids, parallelization in HPC environments requires substantial improvements to manage memory, load distribution and input/output (I/O).

Over the last decade, various numerical schemes have been added to WW3 to allow for the integration of the model over unstructured meshes (WW3DG, 2019). Due to the scalability of the structured grid on a large number of computational cores, it has been used in forecast operation for a long time at the National Center for Environmental Prediction (NCEP), National Oceanic and Atmospheric Administration (NOAA). In

* Corresponding author. NWS/NCEP/Environmental Modeling Center, National Oceanic and Atmospheric Administration (NOAA), College Park, MD, USA.
E-mail address: ali.abdolali@noaa.gov (A. Abdolali).

https://doi.org/10.1016/j.coastaleng.2020.103656
Received 26 November 2019; Received in revised form 23 January 2020; Accepted 25 January 2020
Available online 1 February 2020

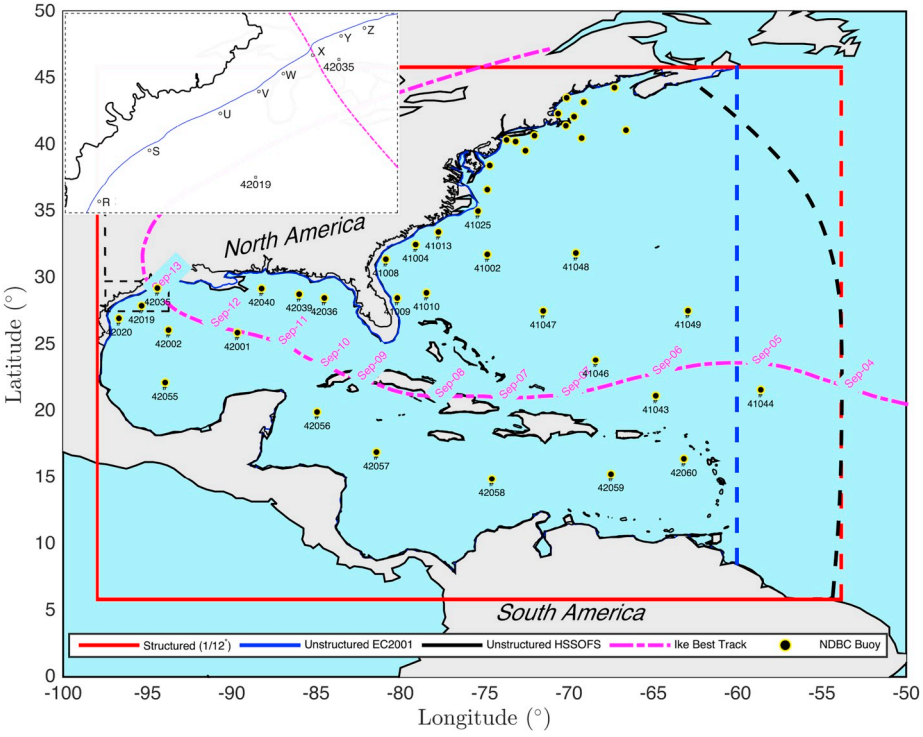

Fig. 1. Numerical domain extents and observations for the east coast of the United States: a structured grid with 1/12 ˚ resolution (red); EC2001 unstructured grid (blue); and HSSOFS unstructured grid (black); The dashed lines show the open boundaries and Hurricane Ike best track and time tags are shown by magenta. NDBC buoy locations are shown in entire domain. The zoom in window shows point source observations near hurricane landfall; NDBC buoys equipped with meteorological and directional wave sensors and quick deployed wave gauges (R–Z). (For interpretation of the references to color in this figure legend, the reader is referred to the Web version of this article.)

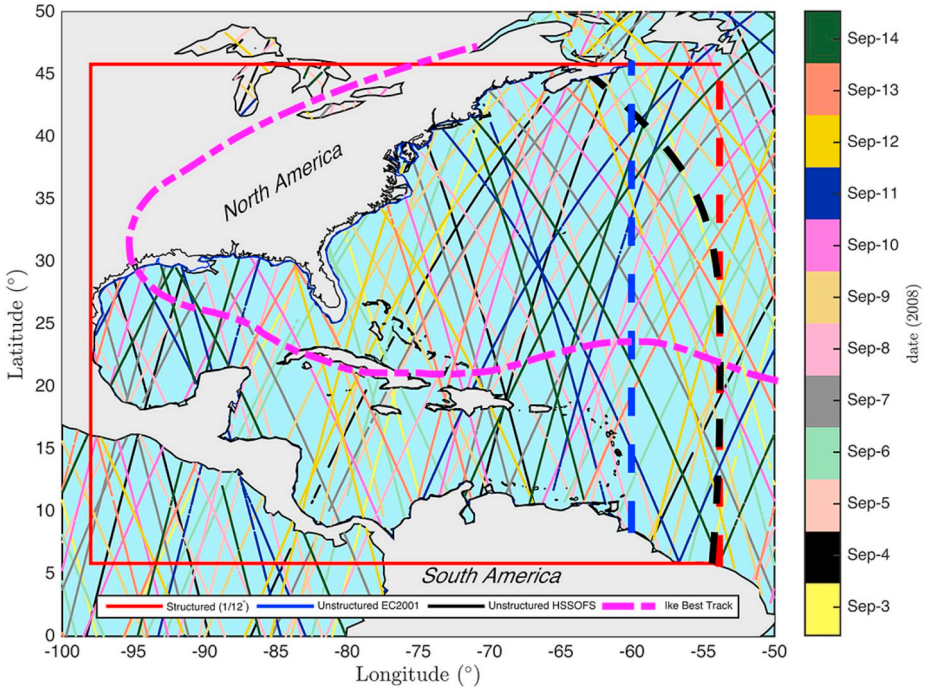

Fig. 2. Satellite altimeters with track date within numerical domains for the east coast of the United States: a structured grid with 1/12 ˚ resolution (red); EC2001 unstructured grid (blue); and HSSOFS unstructured grid (black); The dashed lines show the open boundaries and Hurricane Ike best track is shown by magenta. (For interpretation of the references to color in this figure legend, the reader is referred to the Web version of this article.)

addition, the implemented solvers in WW3 are based on explicit schemes, providing robustness and stability for the model, required for operational environments. However, such explicit solvers have restrictions, such as the number of grid points and minimum grid resolution, limiting further model development. Solving the equations with explicit schemes in WW3 on triangular unstructured grids requires a trade off between spatial resolution and computational resources. For operational applications, this limits the resolution to about 200 m in coastal waters (NOAA ESTOFS Atlantic Storm Surge Model Guidance). In addition, increasing the grid resolution in coastal areas, where most of wave transformation takes place, leads to a significant decrease in time step and subsequent reduction in performance.

The downscaling problem and the discretization of coastal areas, which are fractal geometries, was already recognized by Benoit et al.

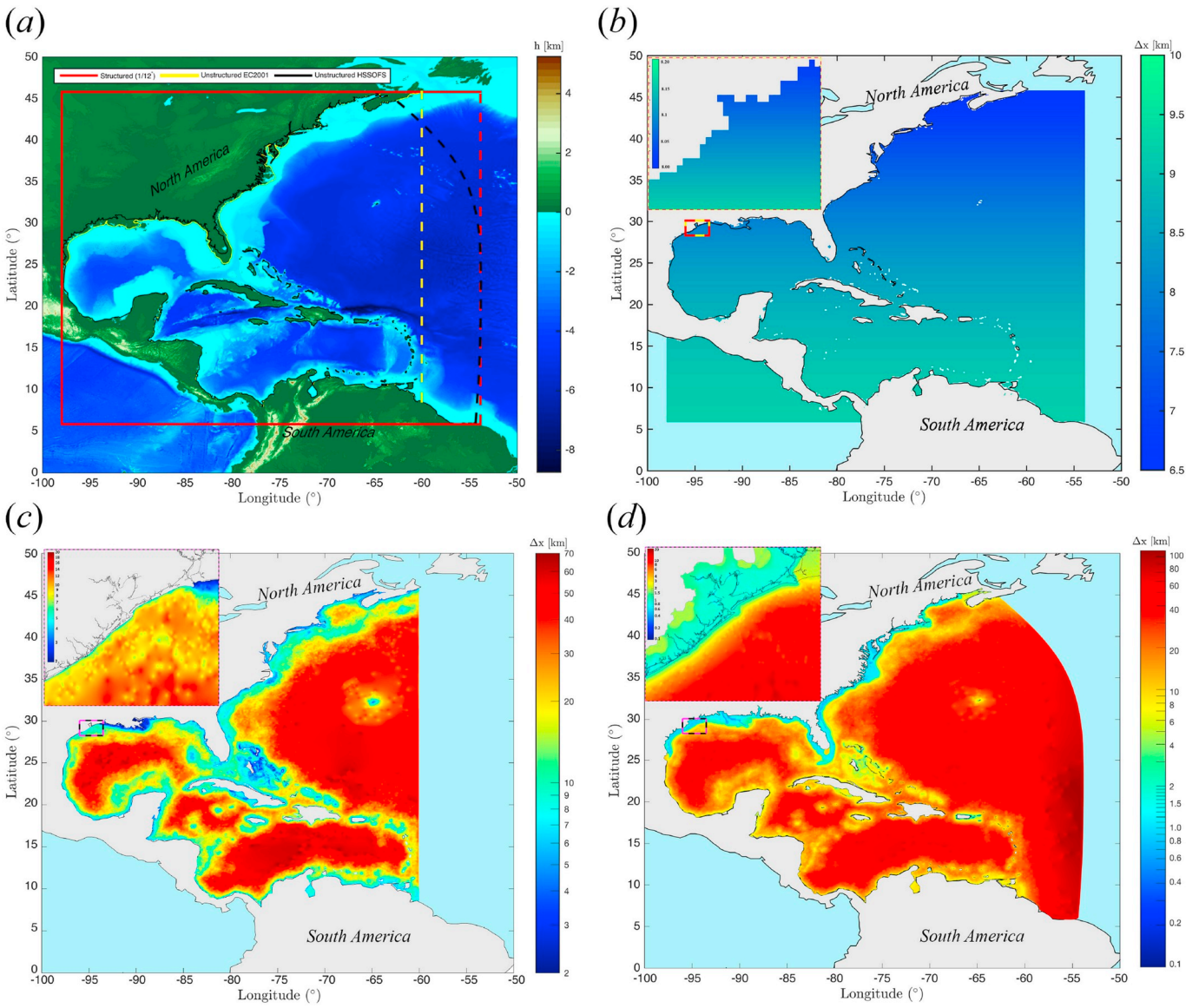

Fig. 3. Topo-bathymetric data (a) and grid resolutions for three grids with a closer view at Hurricane Ike landfall location, Gallveston, TX: Structured grid with 1/12° resolution (variable resolution in km) (b); Unstructured grid EC2001 with ~250×10^3 nodes (c); Unstructured grid HSSOFS with ~1.8×10^6 nodes with inundation extent up to +10 m MSL (d).

(1997) in the TOMAWAC model. The implemented scheme in the aforementioned model utilizes an semi-lagrangian approach, with its benefits and drawbacks (see e.g. Roland (2009)). Following Benoit et al. (1997), Liau (2001) developed the 1st version of the so-called Wind Wave Model, which utilizes implicit schemes on unstructured grids based on Crank-Nicholson Taylor Galerkin methods, within a fractional step approach as used in WW3 for structured grids. The validation study of this work was published in Hsu et al. (2005) and furthermore Roland et al. (2005). In this way the 1st implementation of unstructured grid schemes for the Wave Action Equation (WAE), applying implicit schemes, was presented in Liau (2001). Independently, Sørensen et al. (2005) implemented explicit unstructured grid methods based on the Finite Volume approach into the MIKE21 system based on a local time stepping scheme in order to circumvent the severe time step constraint given by the CFL number. Later on, Roland et al. (2006) and Zanke et al. (2006) introduced the framework of fluctuation splitting methods for the WAE and further developed the WWM, which ultimately led to the development of the WWM-II in Roland et al. (2008). This work incorporated and validated explicit and implicit fluctuation splitting schemes for the WAE. The WWM-II was further developed and coupled with 2D and 3D flow in Roland et al. (2012), where the schemes have been parallelized within the domain decomposition technique. At the same time, similar efforts have been undertaken by Zijlema (2009), where the structured scheme of Simulating Waves Nearshore Model (SWAN), which is fully implicit and does not rely on any kind of splitting of the equations, was reformulated in terms of triangular unstructured grids in geographical space. The SWAN model was further coupled with ADvanced CIRCulation model (ADCIRC, Luettich et al., 1992) and tested for Hurricane Ike, 2008 (Hope et al., 2013). The scalability of SWAN model has been demonstrated to +9000 computational cores using a domain decomposition algorithm (Dietrich et al., 2012).

Numerical modeling of coastal circulation and storm surge, especially near urbanized areas, has gained attention due to the increase in frequency and destructiveness of severe events (e.g., Hurricanes Katrina, Ike, Sandy, Irma and Maria). Advanced models of wind, waves and surge are required to resolve the physics properly, considering small-scale geometries (~20–50 m), high-resolution hydrodynamic, atmospheric forces and physical properties (bed and vegetation roughness). Recent

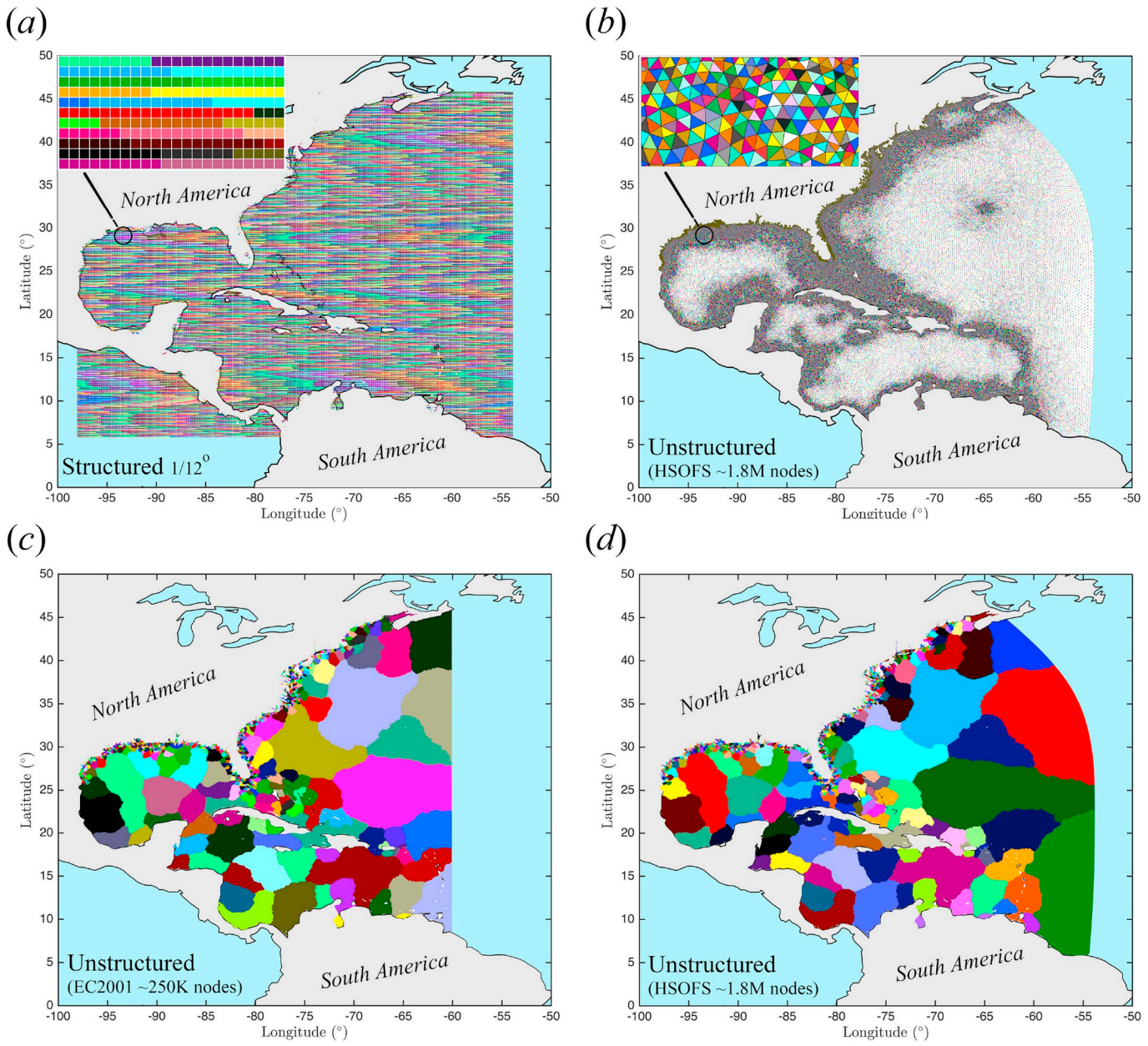

Fig. 4. Schematic view of card deck (top row) vs. domain decomposition (bottom row) approaches implemented in WW3 on 720 computational node with colors representing computational cores allocated to grid nodes; card deck for a structured grid (1/12 °) (a) and an unstructured grid (HSSOFS with ∼ 1.8M nodes) (b); domain decomposition for unstructured grid EC2001 with ∼ 250*k* nodes (c) and HSSOFS grid (d). (For interpretation of the references to color in this figure legend, the reader is referred to the Web version of this article.)

advances in coastal circulation shed light on the need to incorporate wave-surge coupling in nearshore regions. Incorporation of water level and current fields from a surge model in the intertidal/littoral zone together with better resolution of the nearshore bathymetry and wave processes clearly improves the modeled wave field due to their significant role in wave breaking, refraction, shoaling and reflection Ardhuin et al. (2009); Mao et al. (2016); Mao and Xia (2017). This problem is more complicated when the model is coupled with atmospheric and ocean circulation models, requiring compatibility with community based coupling infrastructures. Due to the limits in computational resources, proper core/memory allocations should be implemented to achieve the optimum efficiency. There are two solutions within a coupled infrastructure to optimize High Performance Computing (HPC), allocating more computational cores to a slow model or improving the performance of the slower model to balance loading. It is known that ocean circulation models such as Finite-Volume Coastal Ocean circulation Model (FVCOM, Chen et al., 2013) and ADCIRC, which solve nonlinear shallow-water equations, are comparatively faster than spectral wave models like WW3. However, the coupled system requires simultaneous simulation and information exchange between the wind wave and ocean circulation models. This compels us to improve the numerical approach in the wave model following the work of Roland et al. (2012). In this regard, we have implemented a new domain decomposition algorithm in WW3, which allows us to distribute the workload to a large number of computational nodes efficiently in massively parallel environments, overcoming the scalability problem. As a result, high-resolution unstructured grids on supercomputers with millions of grid cells are now possible. Moreover, taking advantage of the new implementations for coupling with other models, WW3 is modified to operate within the National Unified Operational Prediction

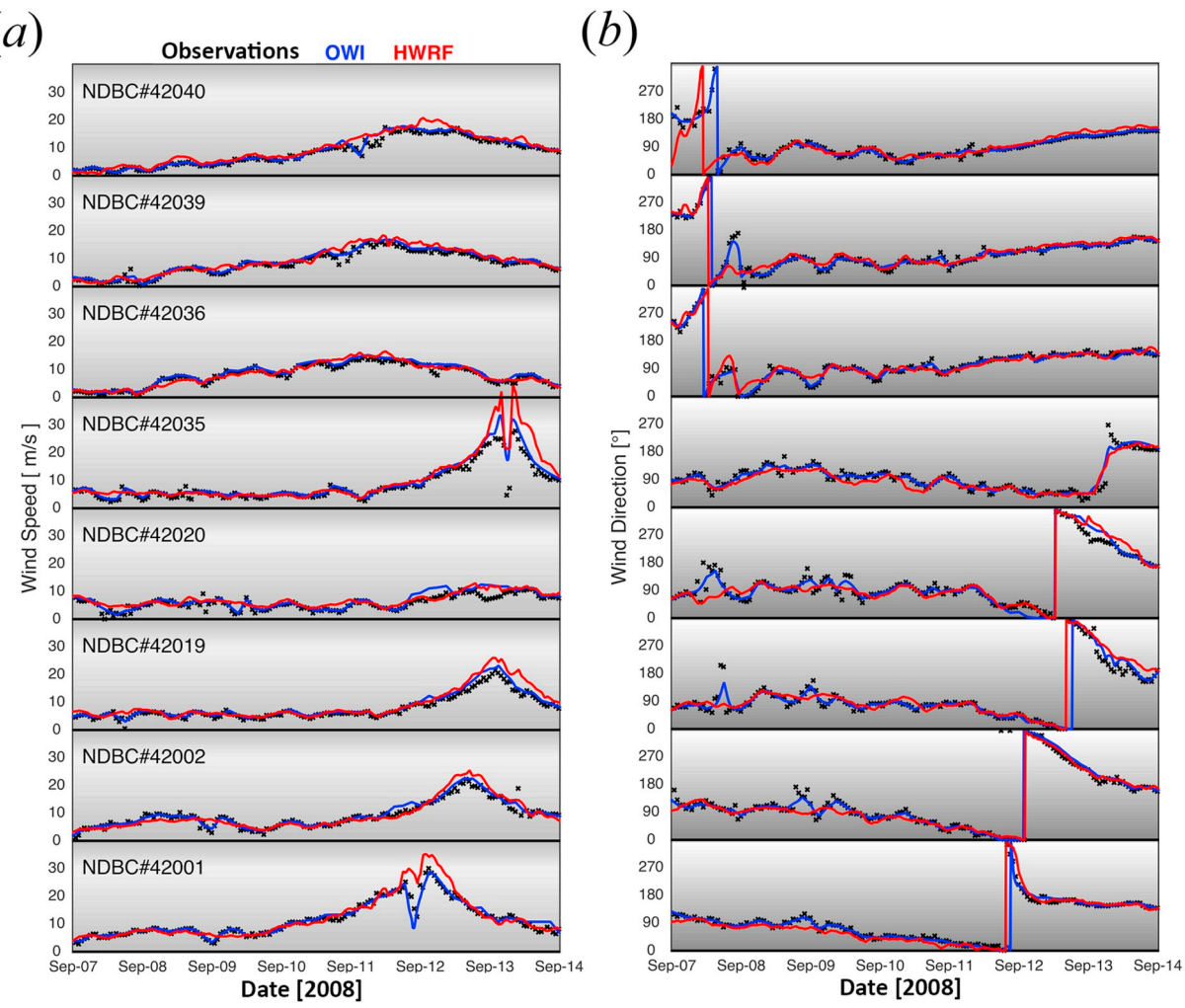

Fig. 5. Atmospheric Model validation at the NDBC buoy locations, OWI (blue) and HWRF (red) versus observations (black): (a) Wind speed (b) Wind direction. *All model configurations and results are pre-decisional and for official use only.* (For interpretation of the references to color in this figure legend, the reader is referred to the Web version of this article.)

Capability (NUOPC) framework (Moghimi et al., 2019), which in turn is based on the Earth Systems Modeling Framework (ESMF) (Theurich et al., 2016).

Unlike explicit schemes, a newly implemented implicit scheme allows us to refine the nearshore region down to street level resolution (~ 10 – 50 m), giving us an opportunity to resolve nearshore physics via dynamic interactions between multiple models, leading to more accurate model outputs (WW3DG, 2019). This scheme integrates the wave action balance equation efficiently in time, and solves all propagation dimensions without any splitting between the various dimensions. This new scheme integrates the source terms directly using a block Gauss-Seidel solver and linearizes them based on Patankar rules or simple Picard iteration, thus avoiding splitting errors in the fractional step method. Therefore, the model can resolve offshore and nearshore physics at once with larger dynamically adjusted time steps compared to the time steps for explicit schemes which are limited by the Courant number (see WW3DG (2019) for more details).

In this work, we have performed a validation study that compares the wave model results using the implicit scheme on various unstructured grids (~2 km and ~200 m resolutions near the US East Coast) with adequate eastward extent, allowing for appropriate generation of hurricane waves from winds over a large region, with the results using a regular grid with ~10 km spatial resolution, as well as with the results of the default explicit splitting scheme. The extreme conditions during Hurricane Ike, which made landfall at Galveston, Texas, allows us to evaluate the model capabilities in detail. The model results are compared with satellite altimeter data for significant wave height, with buoy observations from the National Data Buoy Center observatories (NDBC buoys) operated by NOAA and with quick deployed gauges in shallow regions, ~10 m depth, near the hurricane landfall (Kennedy et al., 2010a). The validation results for the investigated scales show identical results between implicit and explicit methods on unstructured and structured grids in deep water, and superior results from the implicit scheme in nearshore regions where the structured grid does not resolve the coastline and geographical features properly. WW3 performance as analyzed in this manuscript with different combinations of parallelization algorithms and numerical solvers highlights the superiority of each of the aforementioned combinations in term of efficiency and accuracy for the minimum resolution and size of unstructured grids.

This paper is arranged as follows. Section 2 provides a brief overview of the case study, Hurricane Ike. Section 3 describes the point source and satellite observations for model verification. The characteristics of model grids, including a structured and two unstructured grids, are described in Section 4. In Section 5, we describe the new numerical solvers and parallelization algorithm in the wave model. Section 6 describes atmospheric forcing, Oceanweather Inc. (OWI) and the Hurricane Weather Research and Forecasting (HWRF) model, validation and statistical analysis. A detailed description of WW3 sensitivity to atmospheric forcing, grid resolution, numerical schemes, parallelization methodologies, time stepping, model performance and scalability

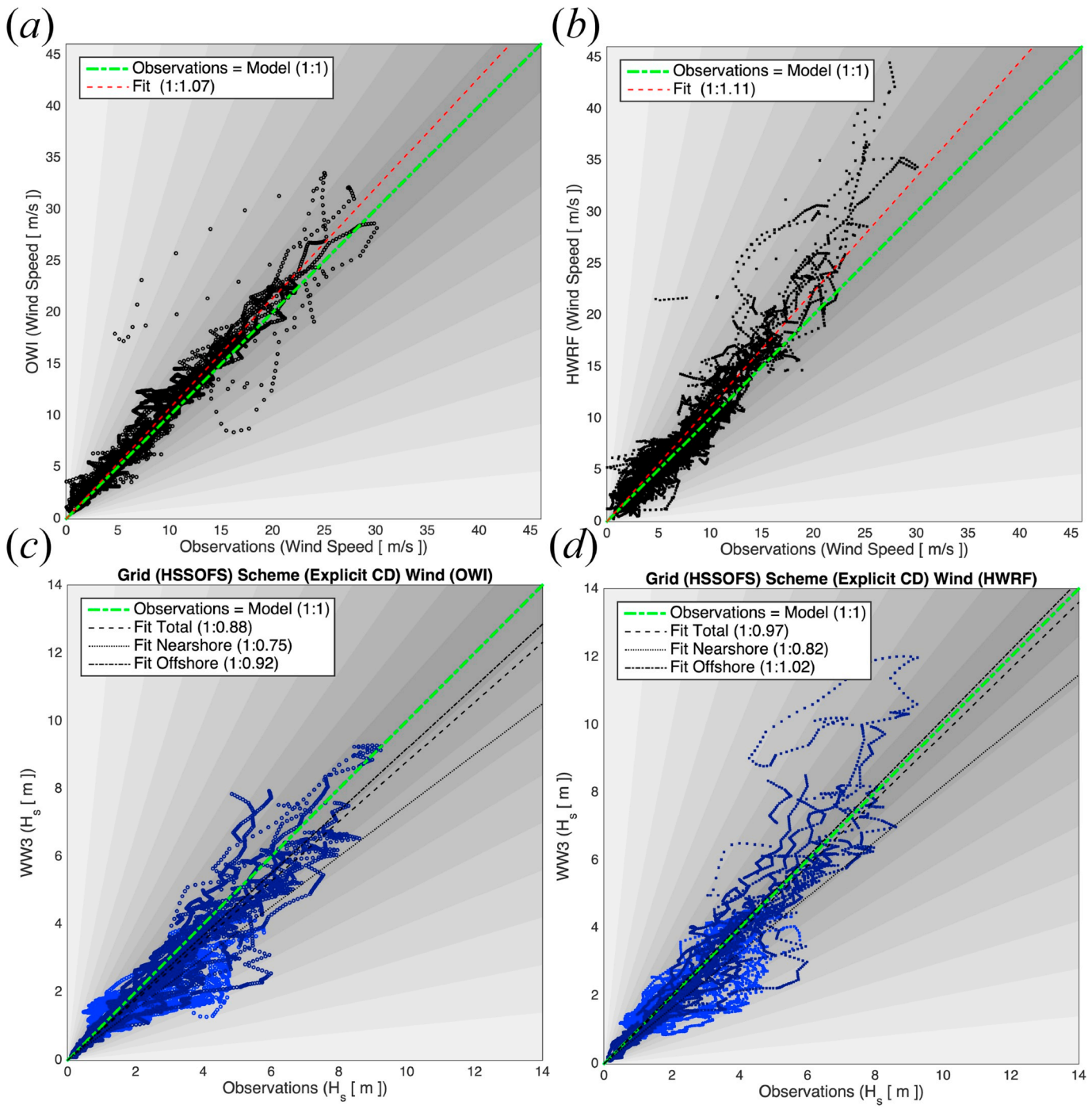

Fig. 6. Linear regression comparison between in-situ data collected at buoy locations and OWI (a), HWRF coupled to the HYCOM, with 3DVar data assimilation and forced with initial and boundary conditions provided by the GFS model (b), WW3 forced by OWI (c) and WW3 forced by HWRF (d) models. The linear regression and model skills are shown in each subplot. The wave scatters are divided into offshore NDBC data (dark blue) and nearshore quick deployed gauges data (light blue). *All model configurations and results are pre-decisional and for official use only.* (For interpretation of the references to color in this figure legend, the reader is referred to the Web version of this article.)

analysis are given in Section 7. Concluding remarks are provided in Section 8.

2. Case study

The case study is Hurricane Ike (September 2008), the ninth tropical storm, fifth hurricane, and third major hurricane of the 2008 Atlantic hurricane season in the U.S. The genesis of Hurricane Ike formed on the west coast of Africa on August 28, and swept westward through portions of the Greater Antilles and North America with significant impact on Cuba. Its wind speed and pressure reached ~ 65 m/s and 935 mb on September 4th. It strengthened to a peak intensity through the Gulf of Mexico and made its final landfall east of Galveston, Texas, on September 13th (Berg, 2009). The maximum surge of 5.3 m was observed at the landfall region (Chambers County, TX). The Hurricane Ike best track with time tag is shown in Fig. 1. The maximum observed waves within the Gulf of Mexico reached ~ a significant height of 9.3 m at NDBC #42001 on September 11 at 6 PM UTC, a few hours before the

Table 1
Atmospheric models' performance at buoy locations and along satellite track in term of wind speed (m/s). *All model configurations and results are pre-decisional and for official use only.*

Obs./Model	Variable	RMSD	σ	CC
Point Source Observation				
Obs.	U_{10}	–	4.38	–
OWI	U_{10}	0.94	4.63	0.98
HWRF	U_{10}	1.84	5.34	0.95
Satellite				
Obs.	U_{10}	–	3.26	–
OWI	U_{10}	1.36	3.24	0.91
HWRF	U_{10}	1.12	3.22	0.94

hurricane eye passed over it. At NDBC gauges closer to the coast and on the east side of hurricane track, waves reached ~ 8 m at noon September 11th, while on the west side of the hurricane track, maximum wave heights of 6–8 m were captured early on September 13th. The WW3 model simulations, which are in good agreement with NDBC buoys, show near 14 m waves along the hurricane track and in mid-Gulf on September 12th. At quick deployed nearshore gauges (Kennedy et al., 2010a), the waves reached ~4.5 m and ~6 m on the east and west sides of hurricane track, respectively. These gauges were located at the depth of ~10 m. These large nearshore waves occurred at larger water depths due to the superposition of the forerunner and the following surge. The peak period of observed waves was about 15 s at most of wave observations. Hurricane Ike's wide wind field together with the broad shelf and geographical features of the Louisiana-Texas regions led to generation of significant wave and surge fields that impacted over 1000 km of coastline. Total property damage to Cuba, the Bahamas and other Caribbean islands was about $37.6 billion and $34.8 billion in Texas, Louisiana, and Arkansas. Ike was directly responsible for 103 and indirectly for 64 deaths in Texas (Brown et al., 2010).

3. Observations

The accuracy of the atmospheric and wave models is quantified at stationary and scattered observations:

3.1. Point source observations

Time series of wind speed, wind direction, significant wave height (H_s), peak period (T_p) and mean wave direction are compared at NDBC buoys located within the Gulf of Mexico where meteorological and wave parameters are collected. In addition, significant wave height and peak period are measured at eight quick deployed gauges, deployed prior to hurricane landfall near Galveston, TX (Kennedy et al., 2010b). The coordinates of NDBC buoys and temporary gauges are shown in Fig. 1.

3.2. Satellite data

In this study, post-processed satellite altimeter data (wind speed and significant wave height), collected by five altimeter missions (ERS2, ENVISAT, JASON1,GEOSAT Follow On and JASON2) are used. Correction algorithms are applied for individual altimeter raw data based on its specific criteria (Queffeulou and Croiz é Fillon, 2012). For wind speed, the calibrated values of normalized backscatter from satellite altimeters (sigma0) and buoy comparison are used for correction (Abdalla, 2012). For significant wave height, a linear correction is applied using buoy comparison (Queffeulou, 2004). The satellite footprints within our numerical domains, consisting of ~90k scattered data points, are shown in Fig. 2 with a temporal color bar. The satellite measures at the speed of ~ 0.05°/s with a sampling rate of ~1 Hz, while the atmospheric and wave model outputs are hourly on variable grid resolutions (OWI on stationary inner nested domains with resolutions of 0.2/0.08/0.02°, HWRF on moving inner nested domains with resolutions of 0.18/0.06/0.02° and WW3 from 1/12° for the regular grid to variable resolutions of the unstructured grids). Therefore, proper projection and averaging are required for the validation and statistical analysis. In this regard, the model outputs are interpolated to the satellite data, where linear interpolation for time and Inverse Distance Weighting (IDW) are used to average between the three and four nearest points for unstructured and structured grids, respectively. Then model and satellite data are sorted in time for each altimeter separately. Finally, the data are averaged every $\Delta x = 0.5$ degrees.

4. Model grids

One structured and two unstructured grids are used in this study, shown in Fig. 3. These grids were selected in accordance with enhancement in grid resolution and size in operational forecast at NOAA due to availability of more computational resources and improvement in the model performance. These grids were tested before going to operation. In this study, the comparisons are performed to validate new implementations in WW3 compared to the well-validated schemes and parallelization algorithms. Further refinement is required in the wave-surge coupling framework to avoid large gradients in radiation stress and unrealistic current velocity fields, exchanged between models, leading to model failure. The topo-bathymetric data and the outer boundaries of each grid are shown in panel *a*, while grid resolutions are shown in panels *b, c & d*. The dashed lines represent open boundaries, where boundary conditions extracted from global simulations are imposed (see Section 6 for more details on open boundary conditions). In panel *b* the structured grid with 1/12° resolution is shown where southeast and northeast corners are located at (98°W, 5°N) and (53°W, 45°N), respectively. The grid resolution near hurricane landfall is ~8 km. Panel *c* shows EC2001 grid, covering the entire Gulf of Mexico and extending into the Atlantic Ocean to the approximate longitude of 60W with 254,565 nodes, 492,179 elements and highest resolution of 2 km along the coast of the US. EC2001 was the previous version of the operational mesh used in the Extratropical Surge and Tide Operational Forecast System (ESTOFS) by National Ocean Service (NOS) at NOAA. In panel *d*, the Hurricane Storm Surge Operational Forecast System (HSSOFS) is shown. HSSOFS eastern extent is a bit further east to the approximate longitude of 55W with 1,813,443 nodes, 3,564,104 elements and highest resolution of 200 m near the coast with inundation potential of up to +10 m MSL. HSSOFS is the current version of the operational HSSOFS and ESTOFS at NOS (Riverside Technology and AECOM., 2015).

5. WW3 developments

New implementation in WW3 for the implicit numerical solver and domain decomposition parallelization algorithm are described in this section. In these regards, the splitting approach was abandoned and the whole equations have been discretized using the framework given in Patankar (1980) for the Navier-Stokes equations, where the left hand side is discretized using 1st order monotone schemes and the right hand side of the equations, the source terms, have been linearized following Patankar (1980). The resulting equation system is assembled in a large matrix, which is stored using the CSR (Column-Sparse-Row) format, neglecting the zero entries in the matrix. The equation system is the solved using a block-gauss-seidel method, which based on the work of Ferziger and Perić (2002), which is parallelized within the domain decomposition context using non-blocking communication over the halo of the various domains. The decomposition was done using ParMetis (Karypis and Kumar, 1999). The full description of new implementations is discussed in WW3DG (2019).

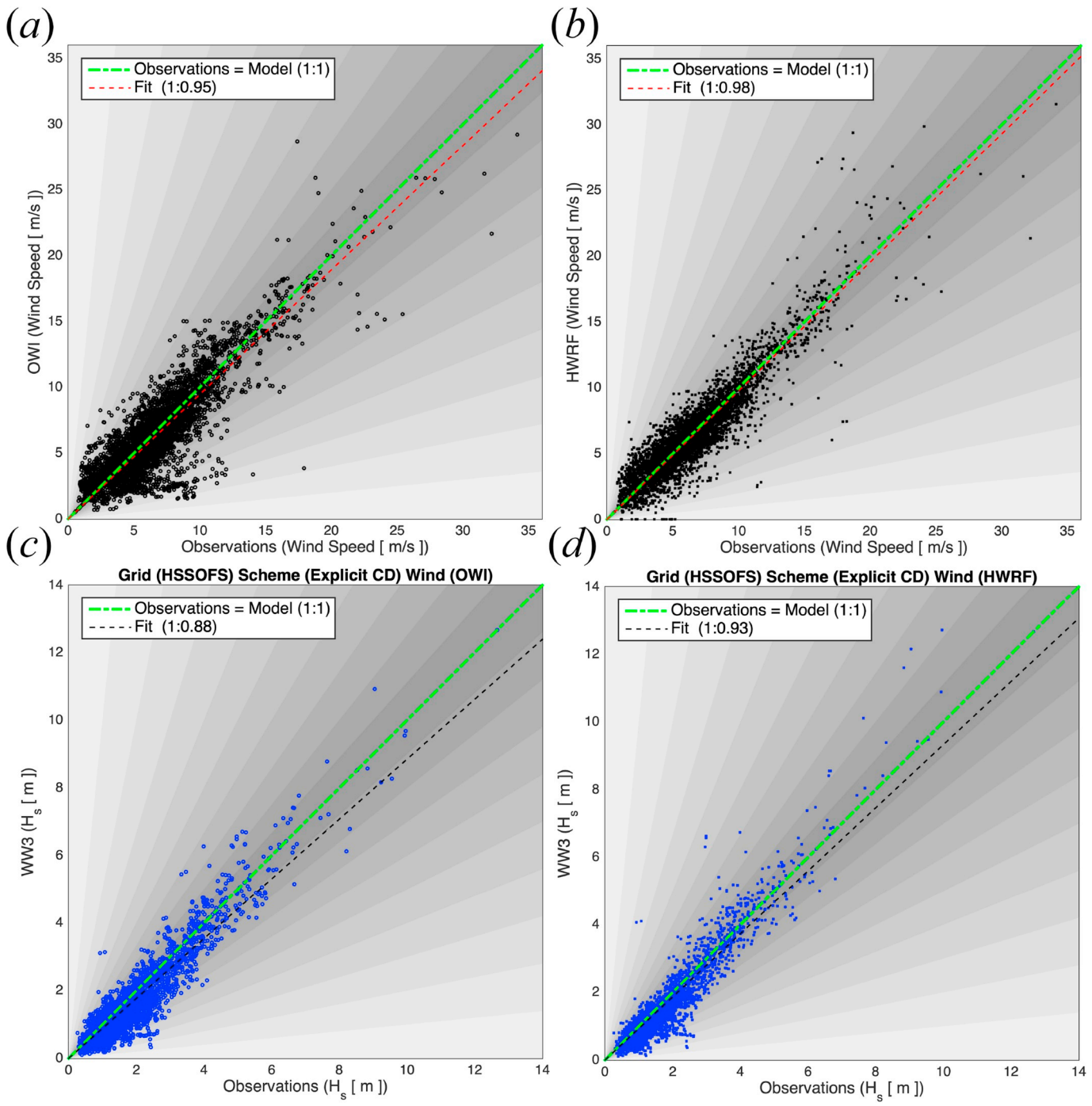

Fig. 7. Linear regression comparison between satellite altimeter data and OWI (a), HWRF (b), WW3 forced by OWI (c) and WW3 forced by HWRF (d) models. The linear regression (blue) and model skills are shown in each subplot. *All model configurations and results are pre-decisional and for official use only.* (For interpretation of the references to color in this figure legend, the reader is referred to the Web version of this article.)

5.1. Numerical scheme

The numerical schemes implemented in WW3 for the triangular unstructured grids are based on Contour Residual Distribution (CRD) for the discretization of the space derivative, adopted to the wave action balance equation similar to the Wind Wave Model-II (WWM-II) (Roland, 2009). With the recent developments, two time integration methods, explicit and implicit schemes, are available for unstructured triangular grids. If the explicit solver is chosen, four time steps are required for global, spatial propagation, intra-spectral propagation and source terms. The solution of the two-dimensional hyperbolic part in geographical space is solved on unstructured grids using the original fractional step method, while the spectral part and the source terms are integrated in a similar way as in the structured version of WW3. In the fractional step approach of WW3, there is also an option for solving geographical advection implicitly. However, it was found by Roland (2009) and Roland and Ardhuin (2014) that this kind approach is very sensitive to the splitting error and consequently leads to a considerable time step dependency as a result of the splitting error between spatial advection, source terms and spectral advection. Note that the fractional step method has a time-step dependency due to the splitting errors. This dependency governs the time stepping, particularly in shallow water

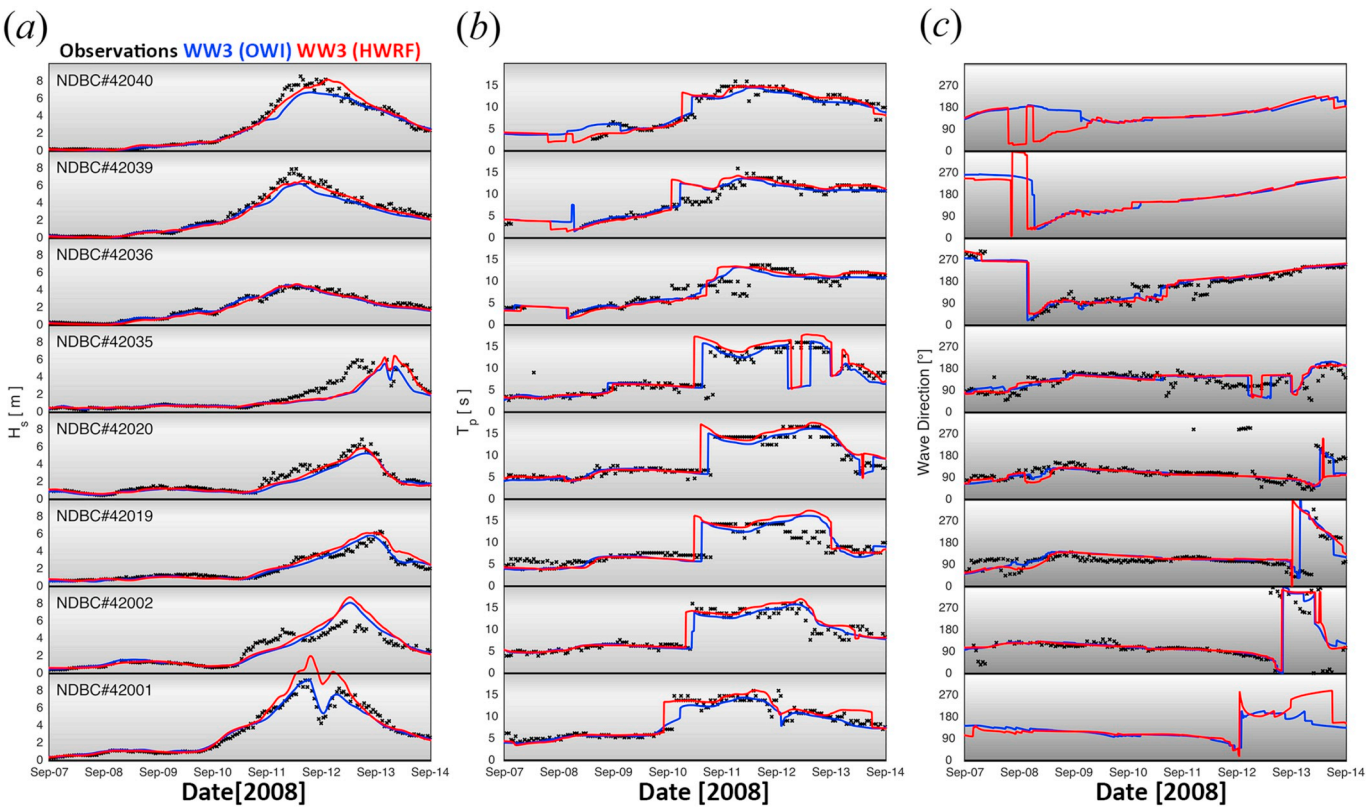

Fig. 8. Wave model validation at NDBC buoy locations, forced by OWI (blue) and HWRF (red) models versus observation (black) with CD parallelization and Explicit solver: (a) Significant wave height (H_s); (b) peak period (T_p) and (c) mean wave direction. *All model configurations and results are pre-decisional and for official use only.* (For interpretation of the references to color in this figure legend, the reader is referred to the Web version of this article.)

(Roland, 2009). Although the time step definition for the unstructured grids with the explicit scheme is similar to that of the structured grids, the number of sub-iterations for the unstructured part is estimated automatically based on the maximal CFL number in the geographical domain. As a result, the minimum grid resolution governs the computational time because it increases the number of iterations for smaller element sizes. Consequently, the explicit scheme becomes inefficient for high-resolution applications. On the other hand, for the implicit method a linear equation system is assembled based on the CRD-N schemes (Roland, 2009). The spectral propagation is solved with simple implicit first-order upwind schemes, the source terms are written in the matrix in the same way as in the dynamic scheme of WW3, and assembling the equation system is based on Patankar rules. Unlike the explicit scheme, only the global time step is required for the implicit scheme, the other time steps no longer affect computations. In this study, we quantify to what extent the time step can be increased without affecting the accuracy of the model both in deep and shallow water.

The model with the explicit scheme requires global, spatial propagation, intra-spectral propagation and source term time steps, while one time step is required for the implicit scheme. In this study, the explicit time steps are chosen as (150, 100, 50, 10 s) while 60 and 600 s are used for the implicit scheme. In all simulations, the model resolves the source spectrum with frequencies between 0.05 and 0.9597 Hz, divided into 32 narrow spectral bands and 36 directions with 10° increment. In order to include the effect of distantly generated swell, boundary conditions are imposed at the eastern open boundary nodes of the numerical domain, extracted from a global simulation. In addition, nonlinear wave-wave interaction using the discrete interaction approximation, DIA (Hasselmann et al., 1985), moving bottom friction (SHOWEX) (Ardhuin et al., 2003), depth-limited breaking based on the Battjes-Janssen formulation (DB1) (Battjes and Janssen, 1978) and reflection by the coast (REF1) (Ardhuin and Roland, 2012) have been used for the computations.

5.2. Parallelization

Parallelization is the efficient work and data distribution on computational processors where the model grid is divided into blocks, and those blocks are allocated to individual processors to do calculations and data communications. The continuity between neighboring blocks is satisfied via proper communications at block boundaries. WW3 has two parallelization methods, card deck (CD) and domain decomposition (DD) in physical space, that overcome computational limits over large grids. A schematic view of these decomposition algorithms is shown in Fig. 4. In the CD method, the land points, where no computation is performed, are excluded. The active points in rows and columns of the model grid are sorted and distributed between processors linearly as in Fig. 4, panels a and b. Unlike structured grids, the indexing of nodes in the unstructured grids is not geographically sequential. Therefore the parallelization looks random in the CD algorithm for the unstructured grids. The efficiency of this method has been proven on structured grids Tolman (2002). The CD method has been used in the operational WW3 for years, for single and multiple grids. Other types of parallelization such as hybrid parallelization techniques have been developed in WW3, which expand each MPI rank into OpenMP threads for further parallelization. In addition, parallelization for shared memory machines using threading has been implemented using standard OpenMP directives (WW3DG, 2019). The parallelization of the unstructured grid schemes is done using either the CD approach (panel b) as done for the structured grids or the DD method (Fig. 4, panels c and d). The DD parallelization replaces the original spectral component parallelization. The spectral-spatial domain is split into several sub-domains. In each sub-domain the spectral component propagation is simulated synchronously and independently, but the information exchange between adjacent numerical sub-domains is performed within the MPI environment. In such an environment, the decomposed N sub-domains can be

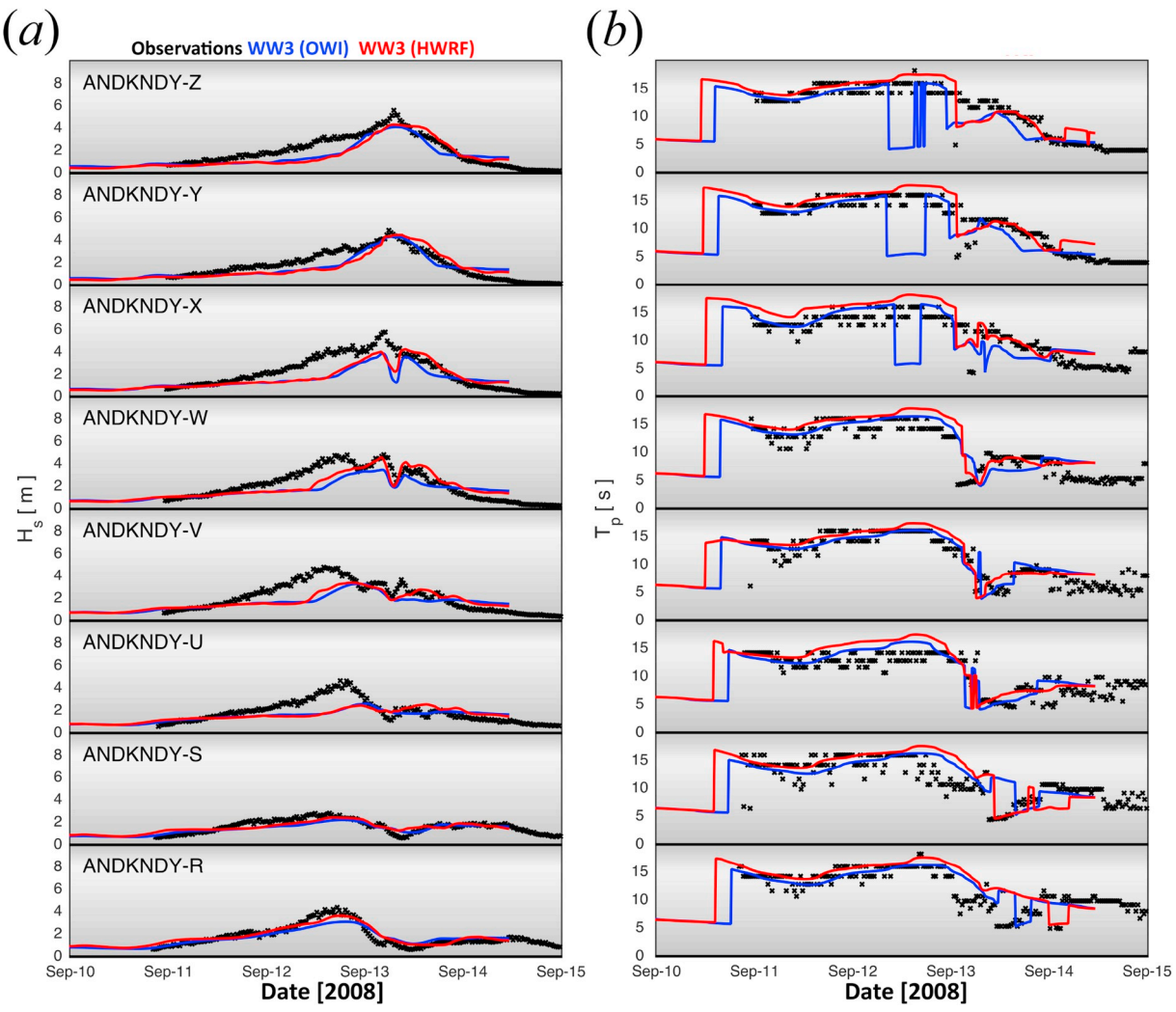

Fig. 9. Wave model validation at quick deployed gauges, forced by OWI (blue) and HWRF (red) models versus observation (black) with CD parallelization and Explicit solver: (a) Significant wave height (H_s) and (b) peak period (T_p). *All model configurations and results are pre-decisional and for official use only.* (For interpretation of the references to color in this figure legend, the reader is referred to the Web version of this article.)

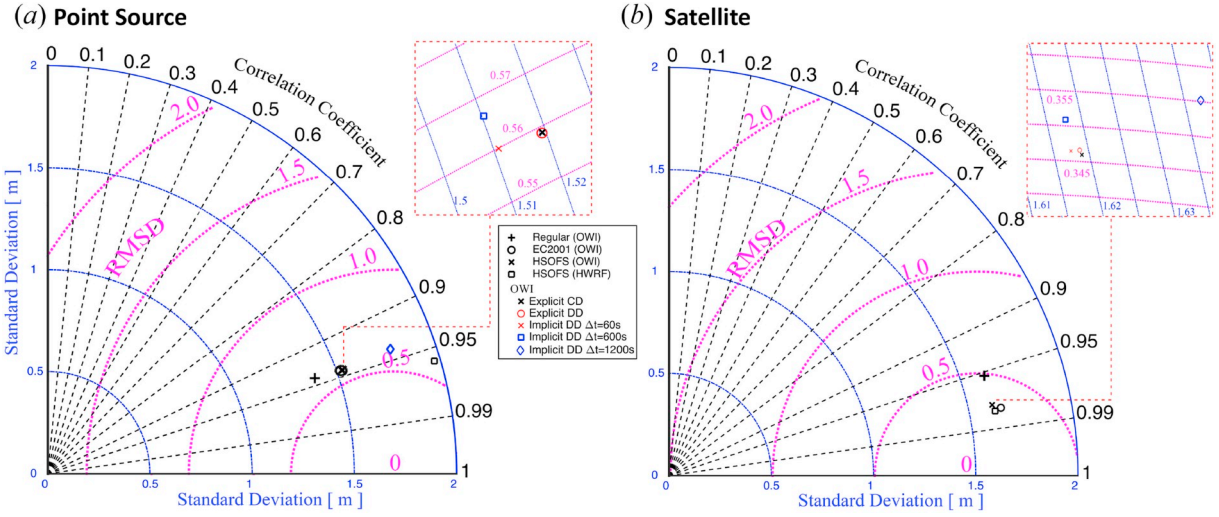

Fig. 10. Taylor diagram for significant wave height, representing modeled and collected data at buoy locations (a) and along satellite track (b) in terms of the Pearson correlation coefficient, the Root Mean Square Deviation (RMSD) and the standard deviation σ. *All model configurations and results are pre-decisional and for official use only.*

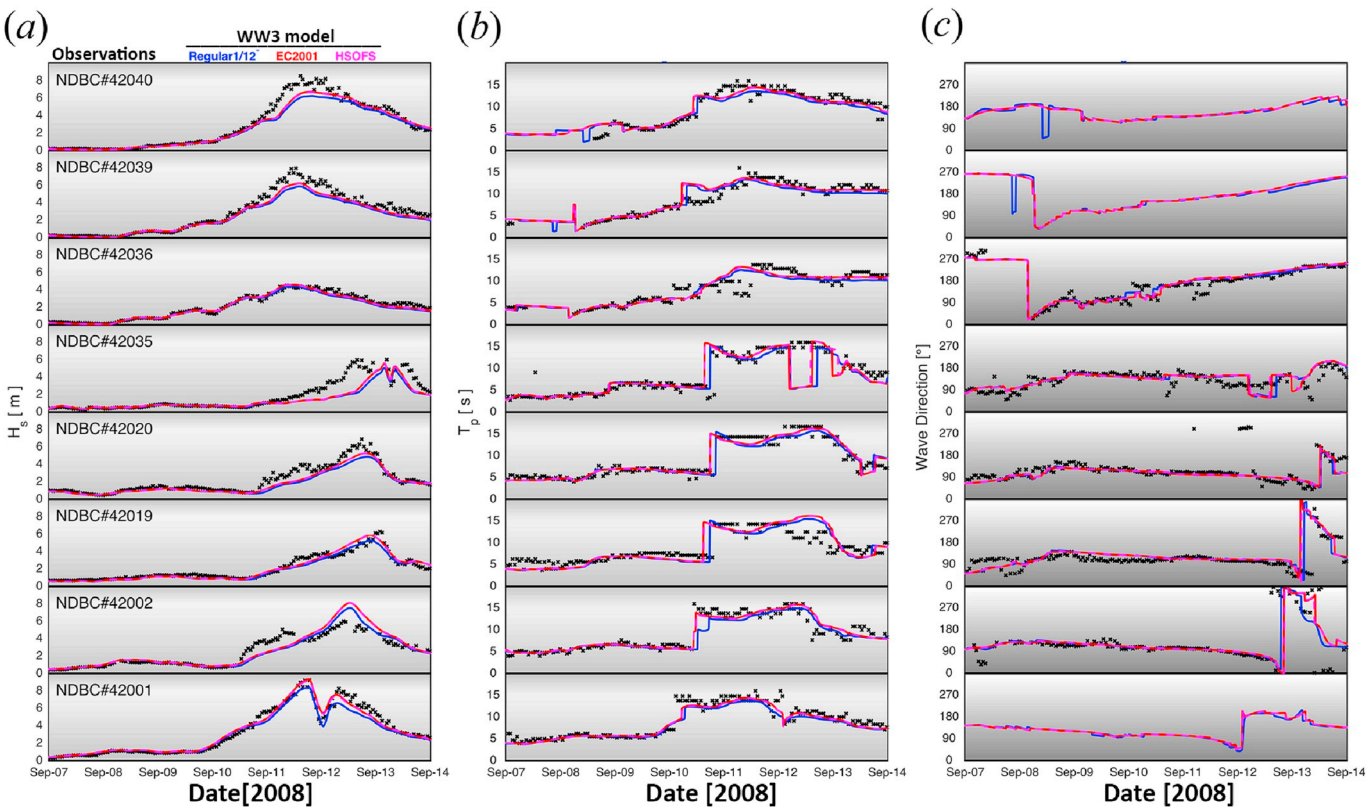

Fig. 11. Wave model validation at NDBC buoy locations, forced by OWI models on the regular 1/12° (blue), EC2001 (red) and HSSOFS (magenta) grids versus observation (black) with CD parallelization and Explicit solver: (a) Significant wave height (H_s); (b) peak period (T_p) and (c) mean wave direction. *All model configurations and results are pre-decisional and for official use only.* (For interpretation of the references to color in this figure legend, the reader is referred to the Web version of this article.)

solved by N processors to achieve the parallel computations. The domain decomposition methods are based on ParMetis (Karypis, 2011), which is a *c* implementation of a parallel graph partitioning algorithm. ParMetis is interfaced using PDLIB (Parallel Decomposition Library) in Fortran. The exchange routines, implemented in PDLIB, do all necessary allocation for the decomposed grids between the various threads based on the decomposition provided by ParMetis. A similar algorithm is implemented in FVCOM (Chen et al., 2013), ADCIRC (Luettich et al., 1992) and SWAN (Zijlema, 2010). Note that the Parmetis based domain decomposition capabilities do not support structured grids in WW3. The full description of the new parallelization algorithm (DD) is discussed in WW3DG (2019).

6. Forcing

We have used two atmospheric forcing data sources to drive the model, Oceanweather Inc. (OWI) (Cox et al., 1995; Cardone and Cox, 2009) and the Hurricane Weather Research and Forecasting (HWRF) model (Gopalakrishnan et al., 2010). Unlike reanalysis products, such as the Climate Forecast System Reanalysis (CFSR) (Saha et al., 2010) and the climate reanalysis ERA5 climatology produced by the European Centre for Medium-Range Weather Forecasts (ECMWF) (Hersbach, 2016), where static data assimilation and numerical schemes are implemented and consequently contain systematic errors on a regional basis and in the extremes, OWI and HWRF are well designed and calibrated for extreme events like hurricanes, making them suitable models for our application. These models provides hourly outputs which are necessary for a rapidly changing hurricane wind fields. The main difference between these two models is that OWI is a hindcast model, therefore all the analyses are performed after the event, taking into account the best hurricane characteristics with post-processed in-situ data. On the other hand, HWRF, as an operational forecast model, constructs an event ahead of the hurricane in real time and adjusts itself every few hours with assimilation of field data. Here, the HWRF model configurations are slightly changed to use known atmospheric conditions based on existing observations (after data quality control) and generate semi-hindcasted wind forcing. In this study and at each time step, the wind field from the highest resolution nested domain is used, extracted from OWI and HWRF models. A detailed description of data post-processing is explained in this section.

The first atmospheric forcing data are provided by OWI, where the model uses a variety of methodologies including the NCEP/NCAR reanalysis wind, statistical downscaling, dynamic downscaling, tropical model overlay and manual kinematic analysis of ocean winds to produce high-quality wind forcing required by ocean response models. The model skill is also evaluated against available in-situ and satellite data. The OWI numerical domain consists of three stationary inner-nested grids that are two-way interactive, Level 1 is the outer box (spanning between 99°W-55°W and 5°N-47°N) with 0.2° resolution, Level 2 with 0.08° resolution as the middle box (spanning between 98°W-80°W and 18°N-31°N) and Level 3 with 0.02° resolution as the finest resolution near the hurricane land fall (spanning between 96.2°W-93.2°W and 27.8°N-30.8°N). The second atmospheric forcing data are generated from the HWRF modeling system empowered by a movable multilevel nesting technology (Zhang et al., 2016). The model grid is triple-nested using telescopic, two-way interactive horizontal grids with resolutions from synoptic at 0.18° as the outer box (spanning about 75° × 75°), to a moving storm box with 0.06° resolution (10° × 10°) and core of about 6° × 6° with 0.02° resolution. These boxes follow the hurricane best track, ensuring the highest resolution around the eye of the hurricane. In this study, we have interpolated the hourly HWRF model outputs from multiple cycles initiated with analysis data and nine forecast time steps.

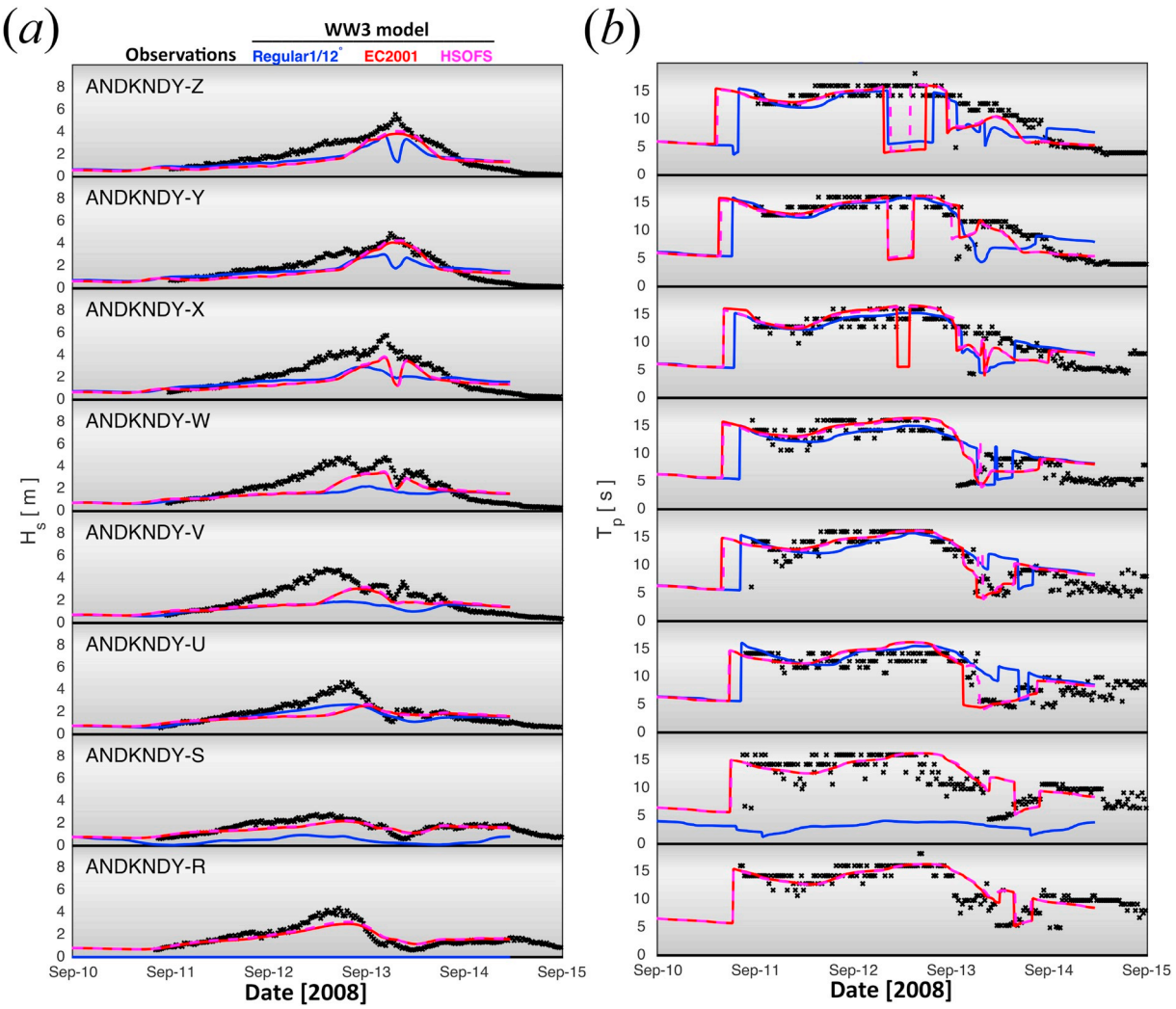

Fig. 12. Wave model validation at quick deployed gauges, forced by OWI models on the regular $1/12^{\circ}$ (blue), EC2001 (red) and HSSOFS (magenta) grids versus observation (black) with CD parallelization and Explicit solver: (a) Significant wave height (H_s) and (b) peak period (T_p). *All model configurations and results are pre-decisional and for official use only.* (For interpretation of the references to color in this figure legend, the reader is referred to the Web version of this article.)

Every 6 h, reanalysis data from the next cycle are smoothly incorporated into the wind field. In the present work, the atmospheric forcing has been validated against NDBC and satellite altimeter data. We extracted wind velocity at 10 m height (U10) from the original GRIB2 output files and saved them in NetCDF format. We used atmospheric fields generated by HWRF coupled to the HYbrid Coordinate Ocean Model (HYCOM) (Chassignet et al., 2007) and three-dimensional variational data assimilation (3DVar) (Zhang et al., 2009) using satellite data. The HWRF model was forced with initial and boundary conditions provided by the Global Forecast System (GFS) with half-degree spatial grid resolution. The animations of wind fields extracted from OWI and HWRF models (provided in supplementary materials) show larger wind values close to the hurricane eye in the HWRF model.

We first compared the U_{10} wind product at point source and field observations via various statistical parameters. Point source data are available at NDBC buoys, as shown in Fig. 5 as time series of wind speed and wind direction. It is clearly shown that OWI is closer to the in-situ data while HWRF overestimates the wind speed (The OWI has skill of 1.07 compared to 1.11 for HWRF as shown in Fig. 6a,b). In addition, at station #42001, where the hurricane track crossed the buoy, OWI captured the peaks and trough accurately. For point source observations, OWI performs better than HWRF in terms of Root Mean Square Deviation (RMSD), standard deviation (σ) and correlation coefficient (CC) for in-situ and model outputs (Table 1). The summary of the statistical analysis is given in Table A.1 (#1, 9) in terms of mean error ($\bar{e}$), absolute error $|e|$, Root Mean Square Error (RMSE), Relative Bias (RB) and skill (see Appendix B for the description of statistical parameters).

In a similar way, we have performed statistical analysis for satellite data where the wind speed is available along the altimeter tracks. In contrast to the analysis for the point source observations, HWRF shows better performance for satellite altimeter data with the skill of 0.98 compared to 0.95 for OWI, as shown in linear regression plots (Fig. 7a,b) and Taylor diagrams, summarized in Table 1. Normal distribution of bias is summarized in Table A.2(#1, 9). The better agreement between the wind field of the HWRF model and the satellite data can be due to the Data Assimilation algorithm embedded in this model, which is based on satellite information (bias of 0.05 m/s for HWRF compared to 0.23 m/s for the OWI model). Unlike HWRF which employs satellite data assimilated basin wide, OWI wind fields are reconstructed on a simplified background field and assimilation is done only in the Gulf of Mexico with the primary focus on the hurricane Ike.

In addition to the surface atmospheric forcing, the global simulations on a regular grid with 0.5° resolution forced by the Global Forecast System (GFS) atmospheric model is performed and the data along the open boundaries of the regional grids are extracted to ensure the long-distance swell is taken into account. This simulation started a month before Hurricane Ike genesis and extended to the end of the storm.

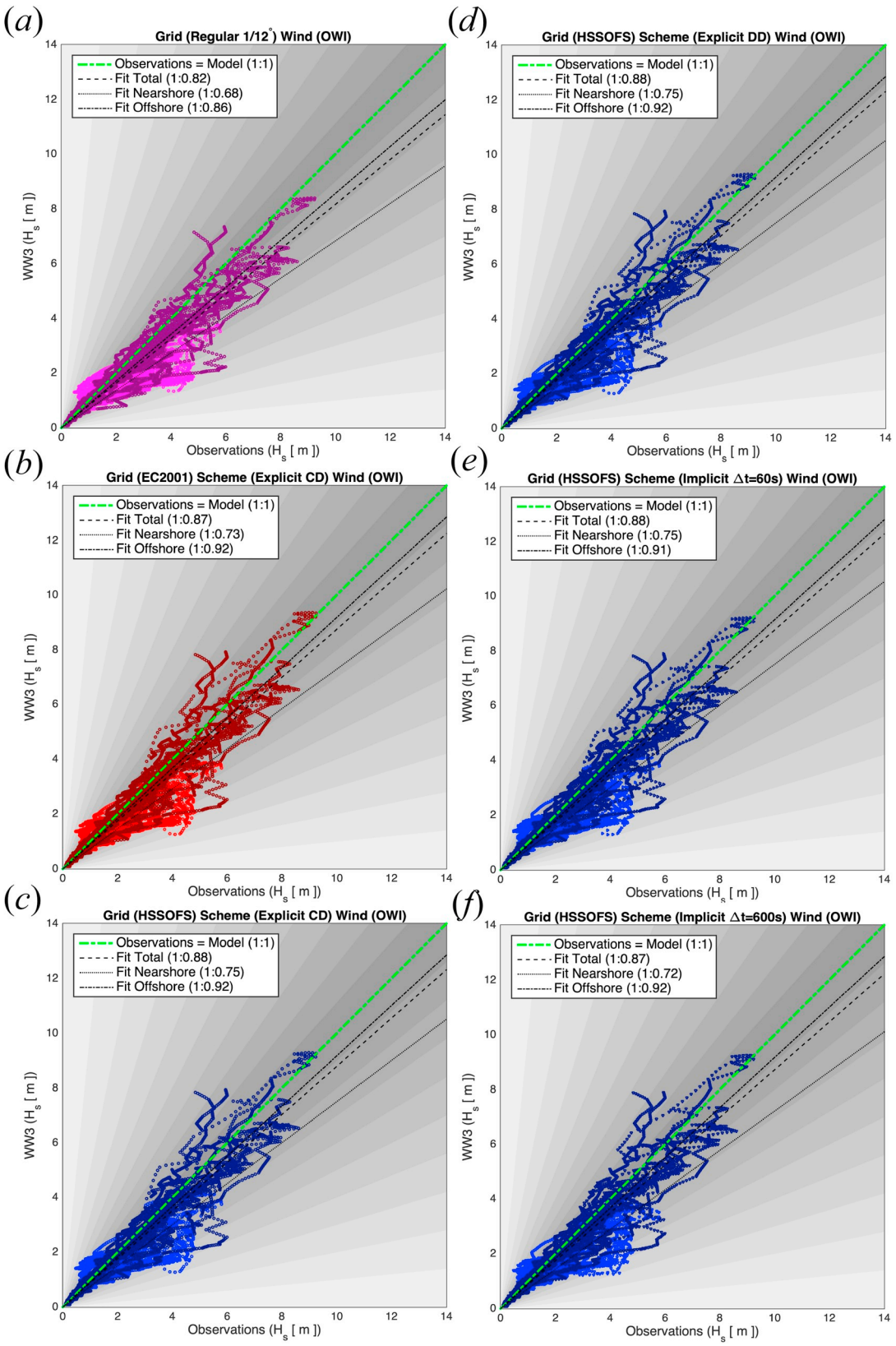

Fig. 13. Linear regression comparison between in-situ data collected at buoy locations and WW3 model forced by OWI on the regular $1/12^{\circ}$ (a), EC2001 (b) and HSSOFS (c) grids using explicit scheme with card deck decomposition for the sensitivity of the model to the grid resolution (Left Panels). The solver schemes and decomposition approaches are compared on HSSOFS grid for explicit scheme with card deck decomposition (c), explicit scheme with domain decomposition (d) and implicit scheme with $\Delta t = 60\ s$ (e) and $\Delta t = 600\ s$ (f) (Right Panels). The linear regression and model skills are shown in each subplot. The wave scatters are divided into offshore NDBC data (dark color) and nearshore data (light color). *All model configurations and results are pre-decisional and for official use only.* (For interpretation of the references to color in this figure legend, the reader is referred to the Web version of this article.)

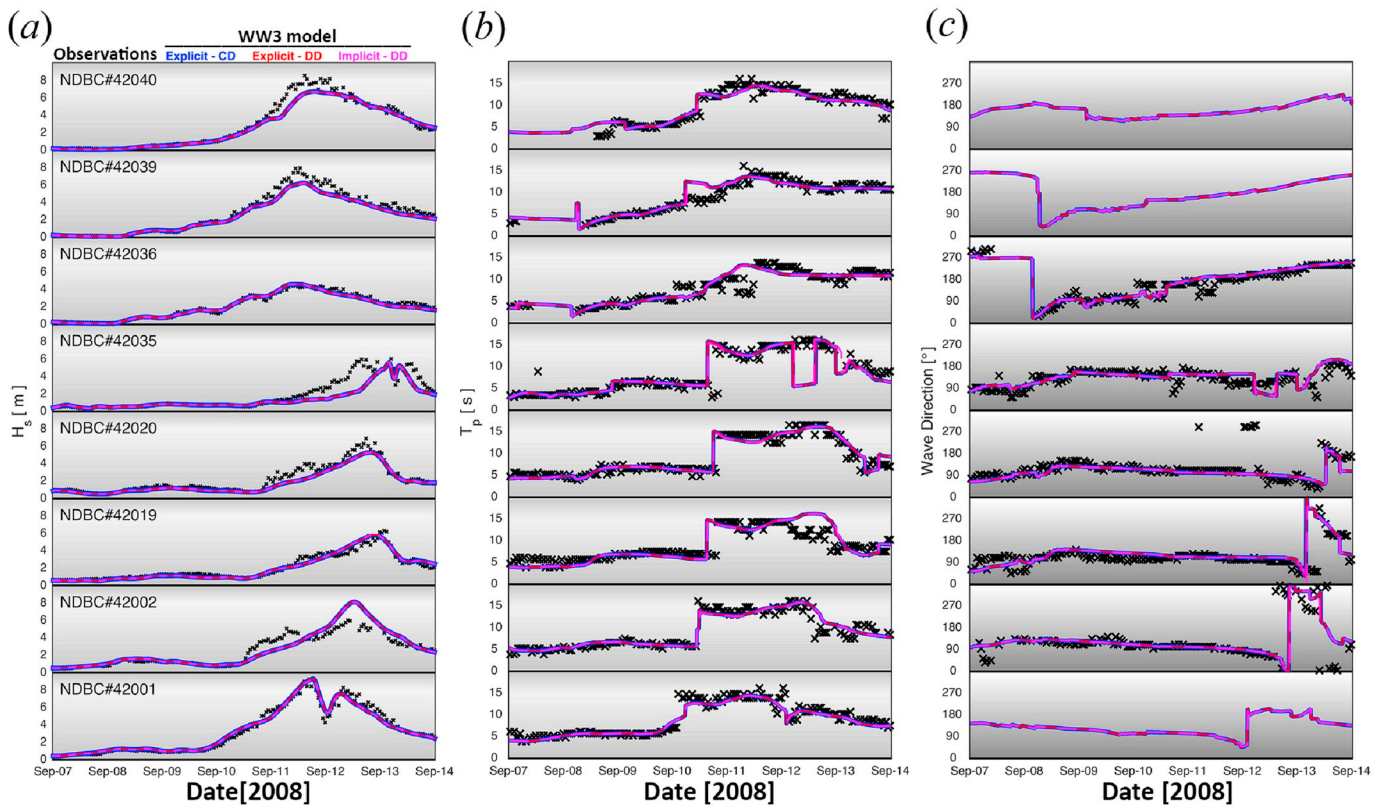

Fig. 14. Wave model validation at NDBC buoy locations, forced by OWI models on HSSOFS grids using explicit scheme with card deck decomposition (blue), explicit scheme with domain decomposition (red) and implicit scheme with domain decomposition (magenta) versus observation (black): (a) Significant wave height (H_s); (b) peak period (T_p) and (c) mean wave direction. *All model configurations and results are pre-decisional and for official use only.* (For interpretation of the references to color in this figure legend, the reader is referred to the Web version of this article.)

7. WW3 validation

In this section, the WW3 performance is evaluated at buoy/gauge locations and along satellite tracks for different atmospheric forcing, grid resolution, numerical schemes, parallelization algorithms and time steps. The evaluation at point locations is done at NDBC buoys locations for significant wave height H_s, peak period T_p and mean wave direction in left, middle and right panels respectively in Figs. 8–9, 11-12, 14-17. The wave direction is not available for the quick deployed gauges, therefore, time series of H_s and T_p are compared. The statistical analysis of H_s is provided for satellite data.

7.1. Sensitivity analysis to atmospheric forcing

WW3 forced by winds from OWI and HWRF is validated on the HSSOFS grid with the conventional parallelization algorithm (CD) and explicit numerical scheme. The time series at NDBC and quick deployed gauge locations are shown in Figs. 8 and 9. At NDBC buoys, the wave model forced by HWRF has larger values for significant wave height as HWRF has larger wind speed compared to OWI. Although the OWI and HWRF performed quite similarly at locations far from the hurricane track, WW3 forced by OWI performed better at buoys close to the track of Hurricane Ike (i.e., NDBC#42001). Note that the discrepancies between model outputs and in-situ data at station #42035 could be due to its movement approximately 25 miles southwest of its original mooring location. A similar pattern is seen for the time series of atmospheric forcing shown in Fig. 5. At quick deployed gauges, both forcings lead to similar results. Comparison of the wave model outputs with observations shows better agreement on the eastern side of the hurricane track (#4204, #42039, #42036, ANDKND-Y and ANDKND-Z). A forerunner surge occurred over a large area prior to the Ike main surge. The area impacted by Hurricane Ike has a wide and shallow shelf, providing proper conditions for generation of Ekman setup when large onshore directed winds to the right of the storm track took place, which started almost a day before hurricane landfall. The forerunner caused early flooding (~ 15 h before the main surge) of coastal regions, and allowed much more effective penetration of flooding into narrow-entranced bays. The forerunner has been reported and discussed in Kennedy et al. (2011) and Hope et al. (2013). Although the scope of this study is to demonstrate the accuracy of new developments in WW3 compared to pre-existing schemes and algorithms, incorporating water level and current fields within a dynamic coupled framework with a hydrodynamic model leads to better representation of in-situ data, especially in nearshore locations. A Taylor diagram shows close correlation coefficients and RMSDs for both forcings but smaller standard deviation for OWI at buoys (Fig. 10(a) and Table A.3(#4, 9)), and similar behavior for all parameters for satellite data (Fig. 10(b) and Table A.4(#4, 9)).

7.2. Sensitivity analysis to grid resolution

The sensitivity of the WW3 model to the grid resolution (as shown in Fig. 3) is quantified at point locations (Fig. 11 for NDBC and Fig. 12 for quick deployed gauges) and along satellite tracks. For this analysis, the CD parallelization and explicit solver are used for different grid resolutions (Regular 1/12°, Unstructured EC2001 and Unstructured HSSOFS). The Taylor diagram and corresponding values are summarized in Fig. 10(a) and Table A.3(#2, 3, 4) for point observations, revealing better performance for the unstructured grids (EC2001 and HSSOFS). In addition, the linear regression analysis and the normal distribution of bias, shown in Fig. 13(a,b,c) and summarized in Table A.1(#2, 3, 4) for the model forced by OWI and (#10, 11,12) forced by HWRF, confirm the mentioned superior model performance for

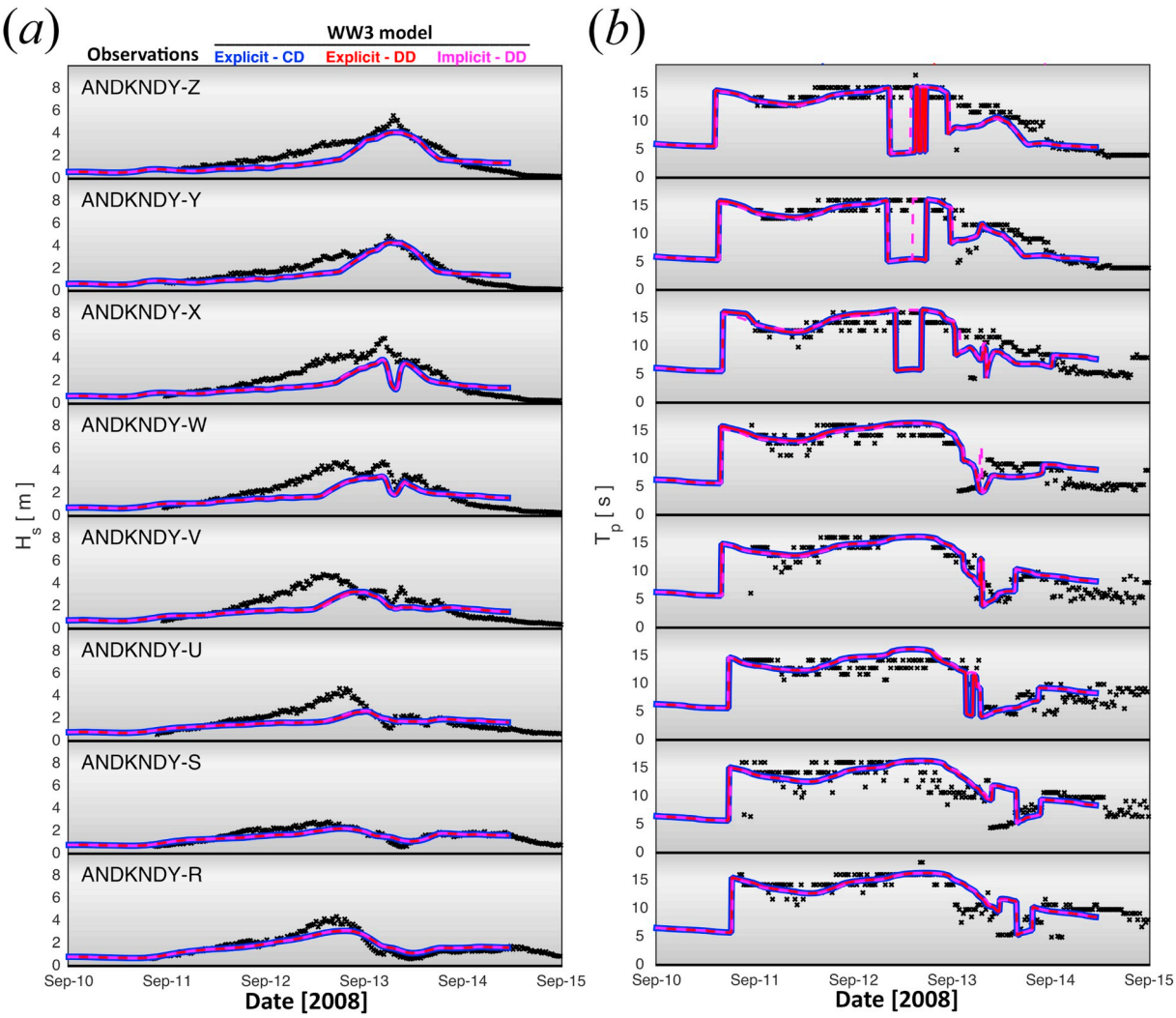

Fig. 15. Wave model validation at quick deployed gauges, forced by OWI models on HSSOFS grids using explicit scheme with card deck decomposition (blue), explicit scheme with domain decomposition (red) and implicit scheme with domain decomposition (magenta) versus observation (black): (a) Significant wave height (H_s) and (b) peak period (T_p). *All model configurations and results are pre-decisional and for official use only.* (For interpretation of the references to color in this figure legend, the reader is referred to the Web version of this article.)

unstructured grids. The comparison at offshore buoy locations (Fig. 11) where EC2001 and HSSOFS have similar resolutions while the regular grid ($1/12^{\circ}$) has higher resolution in mid-gulf, shows visually identical results for the unstructured grids, but slightly different from the regular grid (slightly lower wave heights). At nearshore gauges, shown in Fig. 12, the regular grid does not capture the measurements as well as the results of the model with unstructured grids. This may be due to multiple reasons, including missing the complicated topo-bathymetry and coastline geometries as a result of coarse resolution. Aside from systematic errors introduced by atmospheric inputs as upstream models, the discrepancies between in-situ measurements and high-resolution unstructured grid results in nearshore regions can be improved by improvement in the WW3 physical packages for bed friction, breaking, triad interaction and reflection; incorporating water level and current fields from a hydrodynamic model; and model grid refinement. All aforementioned improvements are under development, thanks to the new possibilities provided by the new parallelization algorithm and implicit solver in WW3 and fully coupled WW3-ADCIRC system. For satellite data comparisons, the Taylor diagram is shown in Fig. 10(b) and Table A.4(#2, 3, 4), a linear regression analysis for the model forced by OWI in Table A.2(#2, 3, 4) and forced by HWRF in Table A.2 (#10, 11, 12). In summary, the simulations on unstructured grids are nearly identical and better than the results extracted from the regular grid setup. It should be noted that most satellite observations are collected in deep water, therefore, the two unstructured grid resolutions are not much different.

7.3. Sensitivity analysis to parallelization algorithm and numerical scheme

The sensitivity of the WW3 model to the parallelization algorithm (card deck vs. domain decomposition) and numerical solver (Explicit vs. Implicit) is investigated next. All the computations are done on the HSSOFS grid. The results of the WW3 model, forced by OWI winds, are shown in Figs. 14 and 15 for the time series verification at the NDBC buoys and quick deployed gauges, respectively, showing visually identical results. Statistical analysis, shown in Fig. 10(a) and for Taylor diagram in Table A.3(#4, 5, 6), confirms identical performance for the explicit and implicit solvers. Linear regression analysis on point observations, divided into nearshore and offshore locations, shown in Fig. 13 (c,d,e), gives skill of 0.88 for all three setups (Explicit with CD and DD; Implicit with DD). The normal distribution of bias and related parameters for point source observations, forced by OWI are summarized in Table A.1(#4, 5, 6) and HWRF in (#12, 13 , 14), confirming previous

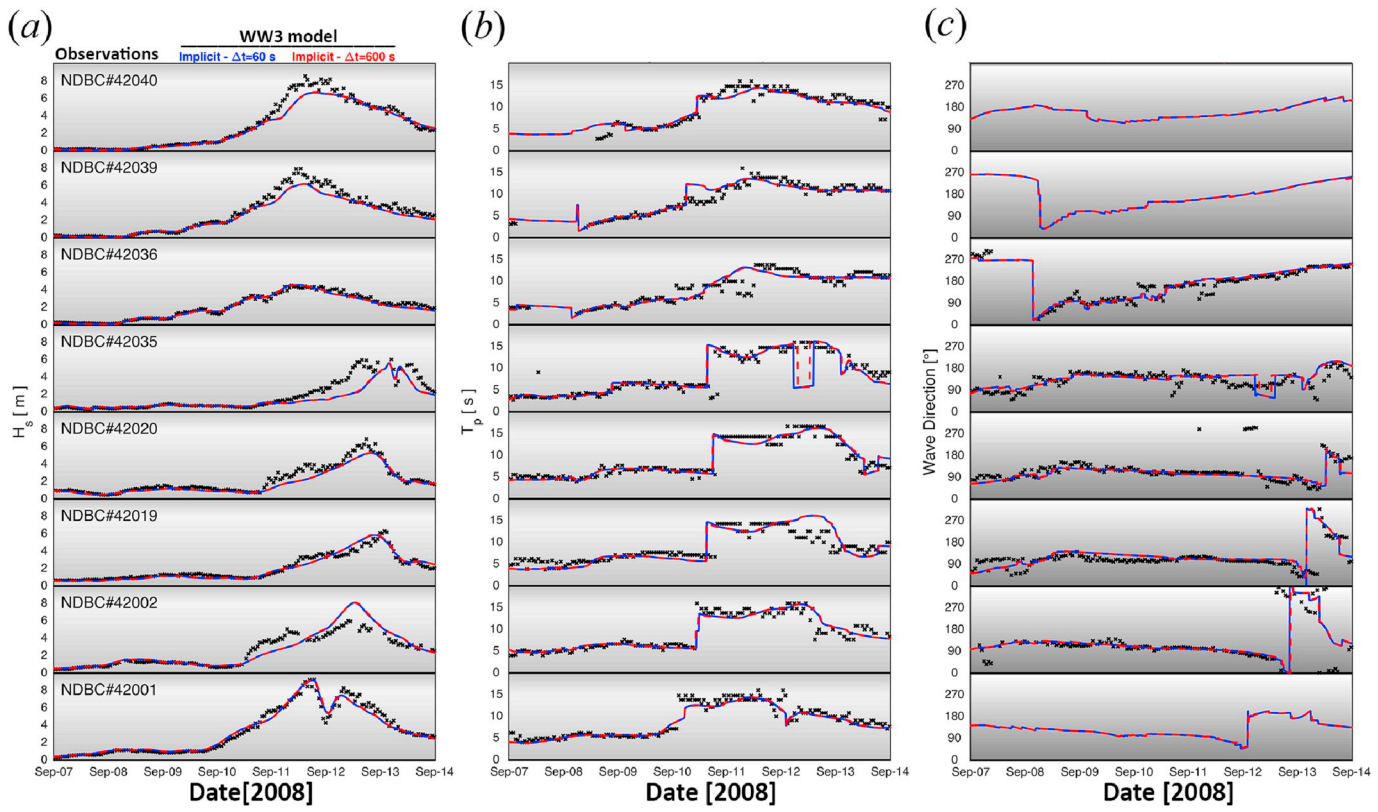

Fig. 16. Wave model validation at NDBC buoy locations, forced by OWI models on HSSOFS grids using implicit scheme with domain decomposition with $\Delta t = 60\ s$ (blue) and $\Delta t = 600\ s$ (red) versus observation (black): (a) Significant wave height (H_s); (b) peak period (T_p) and (c) mean wave direction. *All model configurations and results are pre-decisional and for official use only.* (For interpretation of the references to color in this figure legend, the reader is referred to the Web version of this article.)

model performance. For satellite altimeter data analysis, the Taylor diagram ((Fig. 10(b) and Table A.4(#4, 5, 6)) confirms identical performance (0.98 correlation coefficient). Linear regression analysis for altimeter data and WW3 forced by the HWRF model gives 0.93 skill for all explicit (card deck and domain decomposition) and 0.88 for implicit solvers. The normal distribution of bias and related parameters for field data compared to the model forced by OWI are summarized in Table A.2 (#4, 5, 6) and for HWRF in (#12, 13 , 14). It shows identical performance for all three setups for the model forced by OWI, while the model forced by HWRF shows identical values for the explicit solver with card deck and domain decomposition parallelization and slightly different values for the implicit solver.

7.4. Sensitivity analysis to time stepping

The implicit scheme gives us the opportunity to increase the time step without losing accuracy and reducing computational time. Here, the model outputs are compared for three time steps (60, 600 and 1200 s) for point and field data, where the simulations with 600 and 1200 s time steps took 60% and 75% less computational time than with 60 s time step, respectively. The computations were performed on the HSSOFS grid, with domain decomposition parallelization and implicit numerical solver. The results of WW3, forced by OWI, are shown in Figs. 16 and 17 for the time series verification at the NDBC buoys and quick deployed gauges, respectively, showing visually identical results. Taylor diagram, shown in Fig. 10(a) and in Table A.3(#6, 7, 8), confirms almost identical performance (correlation coefficient of 0.94). Linear regression analysis on point source observation, divided into nearshore and offshore locations, shown in Fig. 13(e and f), gives ~ 0.88 skill for the three setups. The normal distribution of bias and related parameters for point source observations are summarized in Table A.1(#6, 7, 8) for the model forced by OWI and (#14, 15) HWRF, confirming reported model performance. For satellite altimeter data, the Taylor diagram in Fig. 10(b) and Table A.4(#6, 7, 8) confirms identical performance (0.98 correlation coefficient). Linear regression analysis for altimeter data and WW3 forced by HWRF give slightly different performance for the models with 60 and 600 s time steps, but very close results between models with 600 and 1200 s time steps. Note that the energy varies more rapidly as a function of space than as a function of time in the nearshore region and thus having it be a multiple of CFL gives us the ability to resolve nearshore geographical features with a higher resolution grid that would otherwise be possible. The normal distribution of bias and related parameters for field data are summarized in Table A.2(#6, 7, 8) for the model forced by OWI and (#14, 15) HWRF. It shows almost identical performance for both time steps for the model forced by OWI, while slightly different outputs for the model forced by HWRF.

A detailed view of frequency spectra at five gauges consisting of three NDBC buoys (#42001, #42019 and #42036) and two quick deployed gauges (ANDKNDY-Y and S) are provided in Fig. 18 for the observations (a) and model (b). The model outputs are taken from the simulation with the implicit solver on the HSSOFS grid, forced by OWI atmospheric model. The model captures the observed spectrum at NDBC buoys, which are due to an accurate wind forcing (as shown in Fig. 5) and being relatively away from Ekman setup effects. On the other hand, the effects of non-resolved Hurricane Ike forerunner at nearshore gauges are reflected in the early part of the spectral time series, specially at gauge ANDKNDY-Y. Closer to the storm peak, the density spectrum improves and agrees better with the observations. In addition, the higher frequency waves are well captured by the model at shallow water gauges (NDBC #42019 and ANDKNDY-Y and S).

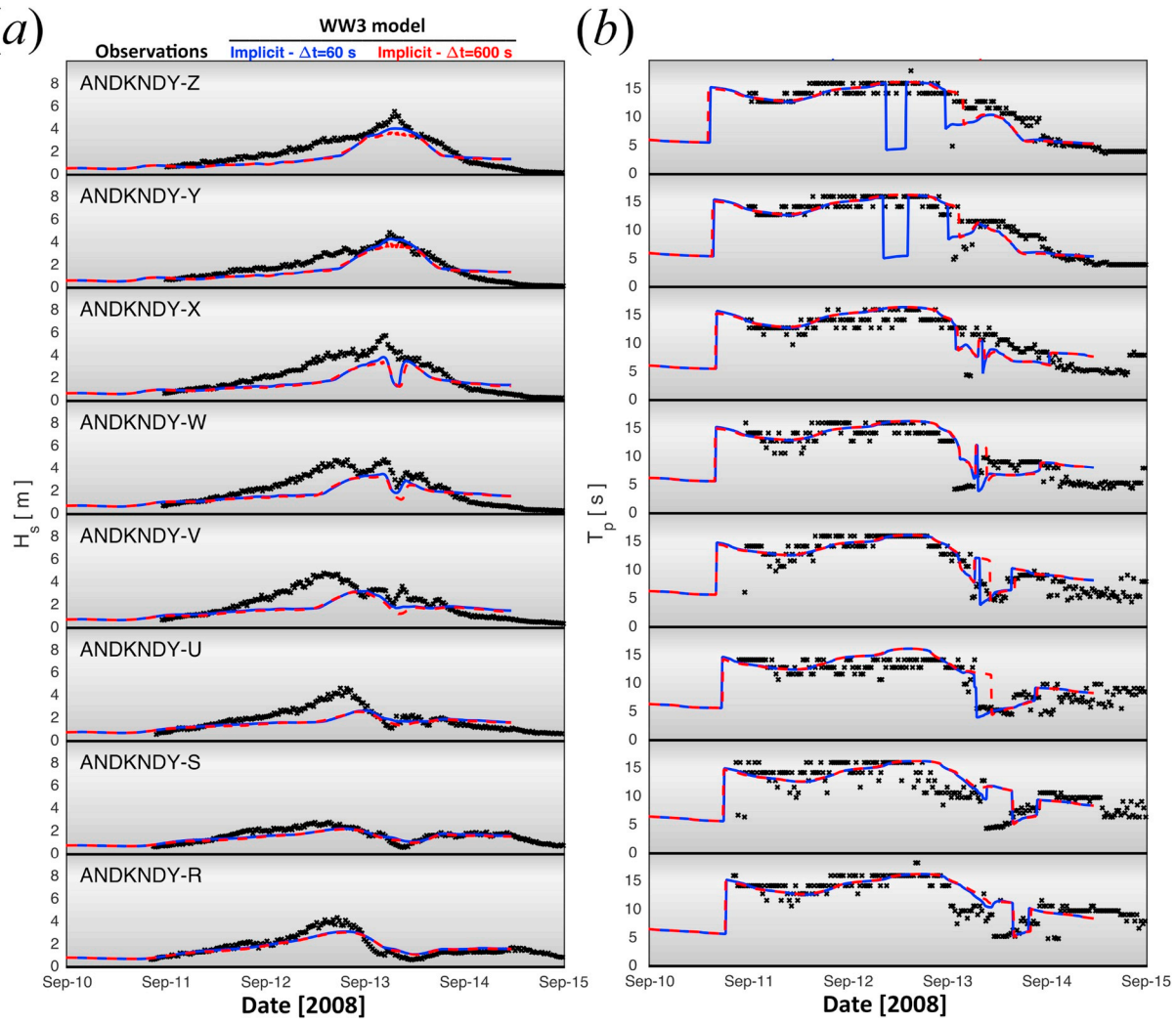

Fig. 17. Wave model validation at quick deployed gauges, forced by OWI models on HSSOFS grids using implicit scheme with domain decomposition with $\Delta t = 60\ s$ (blue) and $\Delta t = 600\ s$ (red) versus observation (black): (a) Significant wave height (H_s) and (b) peak period (T_p). *All model configurations and results are pre-decisional and for official use only.* (For interpretation of the references to color in this figure legend, the reader is referred to the Web version of this article.)

7.5. Model performance and scalability

The model performance (v6.07) has been evaluated on NCEP's HPC's for the pre-existing parallelization algorithm in WW3 (CD) with its explicit equation solver and newly implemented Domain decomposition (DD) algorithm with both explicit and implicit solvers on two regular grids and two unstructured triangular meshes. The extents of these grids are shown in Fig. 1. These grids have be chosen to distinguish the superiority range of each grid and computational limits of each parallelization algorithm. The regular grids have $1/60^{\circ}$ and $1/\ 12^{\circ}$ resolutions corresponding to ~ 2 and 10 km, respectively. The unstructured triangular meshes have 1.8 M and 2.2 M grid nodes with ~ 200 m and ~ 10 m minimum resolutions, respectively. The results are shown in Fig. 19 in terms of non-dimensional computational speed, revealing linear growth in the model performance for various model options and grids with steeper growth for DD (blue, red and magenta solid lines) compared to CD (black, green and gray solid lines) due to communication difficulties on a larger number of computational processors with the CD algorithm. It is clearly shown that the CD performs well for the coarse grid with fewer grid points (black). However, increasing the number of grid points to 2.2 M and decreasing the minimum resolution to ~ 10 m led to a significant slow down in the model performance for the explicit solvers (magenta and gray lines) due to model CFL constraint embedded in explicit scheme on triangular unstructured grids. This limit has confronted WW3 users applying larger grids with very high resolution for a long time. On the other hand, the implicit scheme, as shown by blue line, allows us to resolve the physical processes in nearshore regions with required grid resolution in an efficient way. In addition, the model performance on a regular grid is investigated and shown by dashed lines. Despite the fact that the model performs well for the $1/12^{\circ}$ grid (dashed magenta) and therefore appropriate for global setups, simulation on a very fine resolution regular grid ($\leq 2km$) at such scale is not possible (dashed blue). Fig. 19 shows that the domain decomposition does not have the limit of the CD algorithm, thus larger grids can be distributed on a large number of computational cores greater than $No._{Dir} \times No._{Freq}$.

Note that for the implicit solver, the model proceeds with the time step defined in the setup, however, the computational speed in the implicit scheme is a function of the implicit solver threshold for iteration convergence, therefore the computational time does not drop linearly by increases in the time step. This threshold can be tuned to achieve acceptable results. For this simulation and to achieve good agreement with both offshore and nearshore observations, the implicit solver threshold is defined as 1.E−6 m. For a good agreement at deep water, this number can be chosen larger, however, the nearshore accuracy requires smaller threshold. Although not possible for Hurricane Ike, which lacks adequate shallow water wave observations in the breaking zone

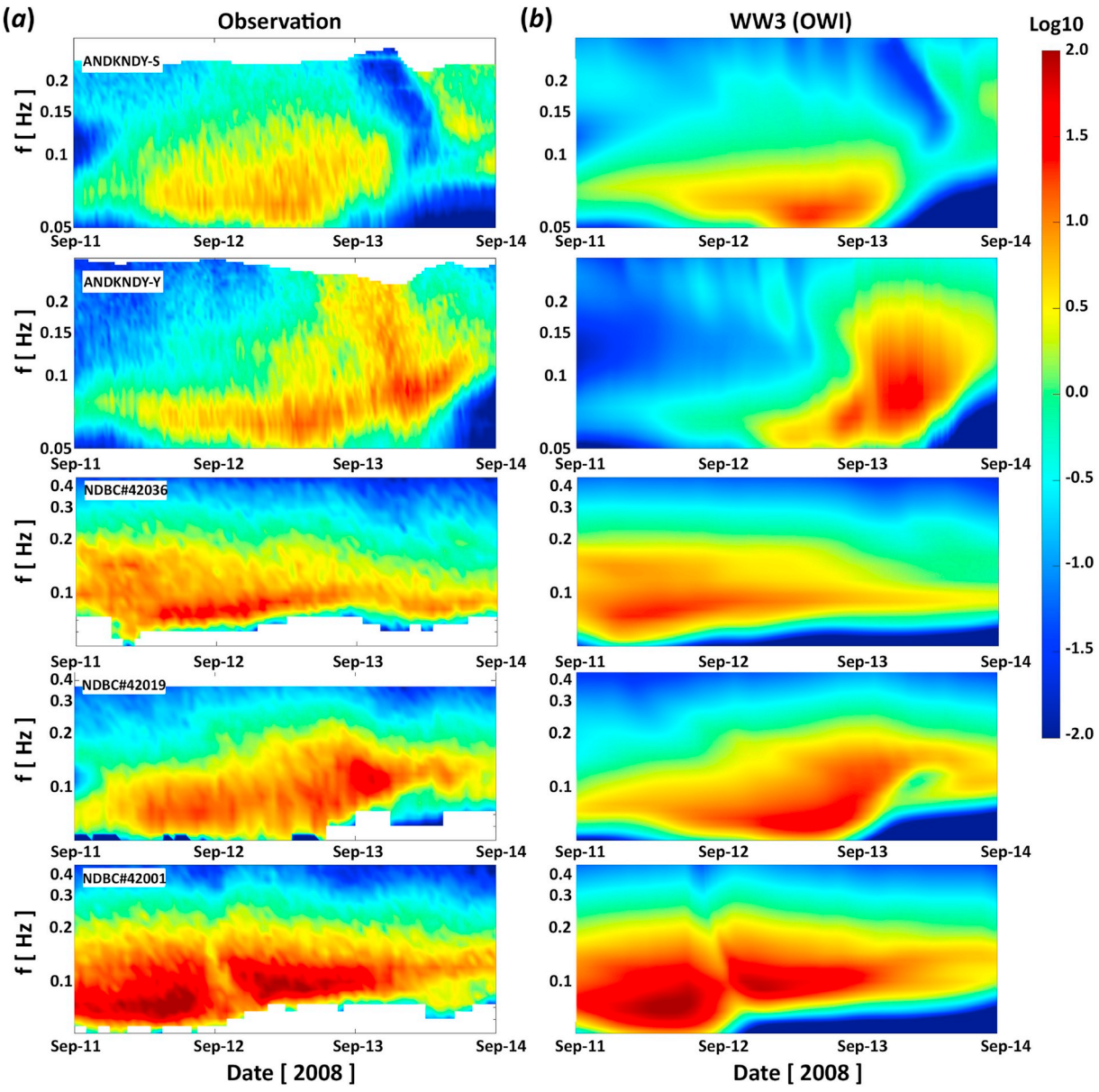

Fig. 18. Frequency spectrum at five selected gauges (3 NDBC buoy and 2 quick deployed gauges) comparing observation (a) versus WW3 simulations forced by OWI (b). *All model configurations and results are pre-decisional and for official use only.*

and overland, such a threshold can be optimized to achieve good agreement with observations. This breakthrough has expanded the limits of WW3 and provides the opportunity to investigate nearshore wave climate on a single triangular grid from coarse offshore to high-resolution nearshore grids instead of multiple inter-nested grids with different resolutions. This analysis draws the limits for each algorithm and scheme and provides a guide for the users to select proper options dependent on the minimum grid resolution. It should be noted that the WW3 numerical solver and parallelization initially were based on the explicit scheme and the conventional CD algorithm on coarse grids, which does not require a large memory. On the other hand, the implicit scheme requires larger memory, and an optimized memory management and input/output (I/O) can potentially improve model scalability and computational speed.

8. Conclusions

In conclusion, we have performed a comprehensive qualitative and quantitative study on the application of WW3 on large-scale numerical domains employing the new parallelization algorithm and implicit numerical solver for unstructured grids compared to the pre-existing parallelization algorithm, domain decomposition, and robust explicit numerical solver of WW3 on both structured and unstructured grids. These new capabilities in the wave model push the limitations of the model, including minimum grid resolution in the present study of ~200 m, maximum number of model grid points (~1.8M) and computational scalability (720 computational cores) based on NCEP's HPCF's. The new domain decomposition algorithm, based on a parallel graph partitioning algorithm, allows us to resolve the nearshore domain and physics with higher resolution, where most of the wave transformations are taking place. Moreover, the wave model is now scalable on HPC environments, therefore the wave model is able to run more efficiently with domain decomposition (DD) and the implicit solver than the conventional parallelization algorithm (CD) and explicit solver on large grids with very high-resolution nearshore elements without a limit on total core numbers (Fig. 19). More broadly, these new features in the wave model enhance the efficiency of wave-surge coupled system (Moghimi et al., 2019). In addition, the implicit Contour Residual Distribution (CRD)

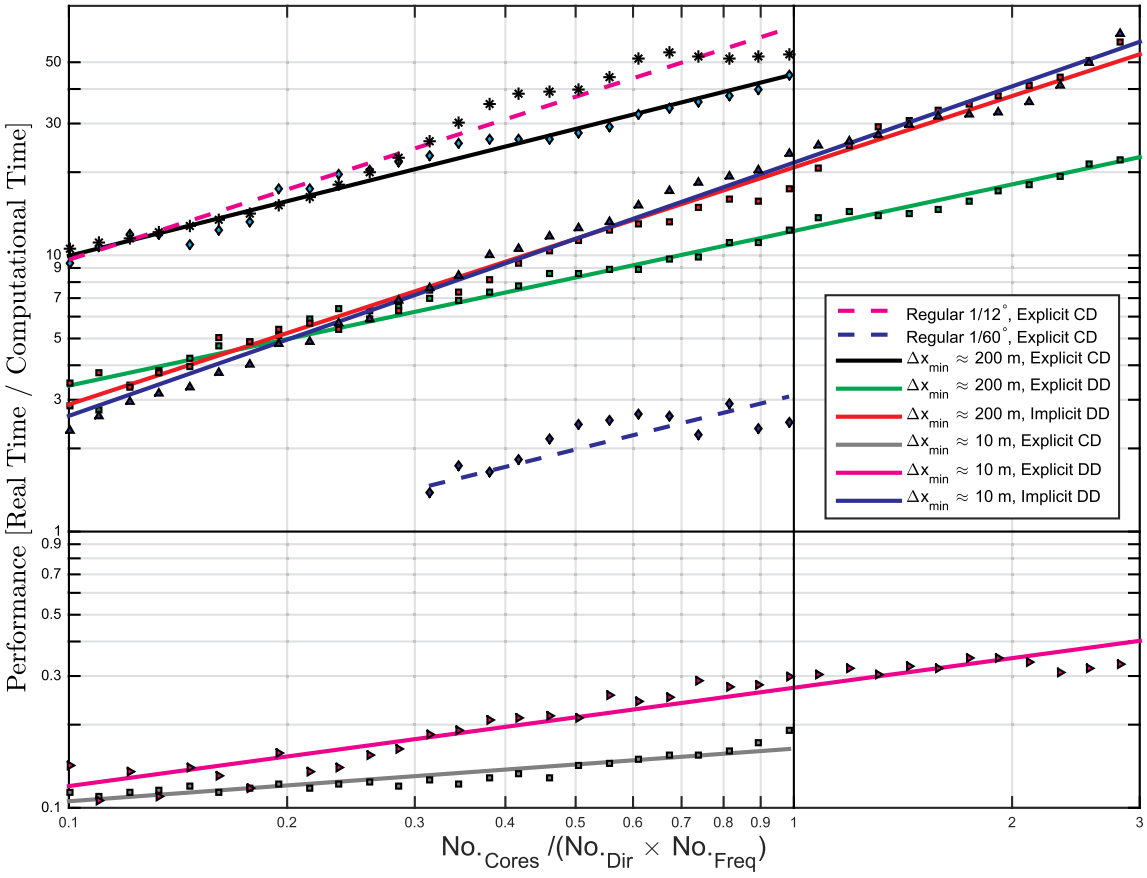

Fig. 19. Model performance (v6.07) on HPC environment and Scalability of WW3 models for CD/DD parallelization algorithms and explicit/implicit numerical solvers for two regular grids with 1/12° and 1/60° resolutions (dashed lines) and two unstructured triangular meshes with 1.8 M and 2.2 M nodes with ~ 200 m and ~ 10 m minimum resolutions (solid lines) respectively. The horizontal axes shows the number of computational cores normalized by spectral and directional resolution. The vertical solid line represents the CD limit ($No._{Cores} = No._{Dir} \times No._{Freq}$). The horizontal solid line represent realtime performance. The tests are performed on NCEP's HPC, Theia, equipped with 2.60 GHz Intel Haswell CPU and 2.67 GB memory/core.

schemes in geographical space in combination with simple first-order upwind schemes in spectral space allow us to increase the model time step, saving computational resources, without losing accuracy with respect to the investigated applications. The new numerical scheme shows better accuracy with respect to the statistics in contrast to the explicit scheme. It is anticipated that the reason for this is the fact that the new implicit solver does not have splitting errors in contrast to the fractional step method used for the explicit schemes.

The case study is Hurricane Ike (2008), generated off the west coast of Africa, entering the Gulf of Mexico with landfall near Galveston, TX. The model performance is evaluated at stationary NDBC buoys and rapidly deployed gauges in the nearshore region and along satellite altimeter tracks. The methodology for spatiotemporal interpolation and averaging of model output and satellite data is discussed in this paper. In this study, two well-known atmospheric models, OWI and HWRF both designed for hurricane modeling, are used to drive WW3. The statistics reveal better performance of OWI at point source observations and of HWRF for satellite wind data. A similar conclusion is given in the downstream wave model, where WW3 forced by OWI captures the characteristics of the in-situ data at buoy locations, while the general analysis shows better WW3 performance along satellite tracks, when forced by HWRF. The migration of the errors, introduced by the atmospheric models reveals similar superiority of the atmospheric model and corresponding wave simulation at stationary or along satellite track observations depends on the data assimilation and bias correction techniques in the atmospheric models. The validation is extended further to quantify the sensitivity of the model to the grid resolution. The wave model shows better performance on high-resolution unstructured grids compared to a regular curvilinear grid, as expected. The different parallelization algorithm (card deck vs. domain decomposition) and numerical solvers (Explicit vs. Implicit) are compared, revealing similar model performance. Lastly, the sensitivity of the implicit solver to the time step is tested, where the model with 60 s time step and an order of magnitude larger time step (600 s) give similar accuracy with 60% less computational time for the larger time step. Further developments are under way to improve the model performance in terms of numerical efficiency, memory usage, parallel scalability and model accuracy, especially in nearshore regions. The need for more work is mostly dictated by the general structure of the code, which does not inherently consider the domain decomposition, and given the multi-grid architecture of the code, which needs to be streamlined to the domain decomposition philosophy.

CRediT authorship contribution statement

Ali Abdolali: Conceptualization, Data curation, Formal analysis, Investigation, Methodology, Software, Validation, Visualization, Writing - original draft. **Aron Roland:** Formal analysis, Methodology, Software, Writing - review & editing. **Andre van der Westhuysen:** Methodology. **Jessica Meixner:** Methodology, Writing - review & editing. **Arun Chawla:** Methodology, Funding acquisition, Project administration. **Tyler J. Hesser:** Methodology, Software, Writing -

review & editing. **Jane M. Smith:** Methodology, Writing - review & editing, Funding acquisition, Project administration. **Mathieu Dutour Sikiric:** Methodology, Software.

Acknowledgement

This work has been supported by the US. Army Corps of Engineers (USACE) and The Consumer Option for an Alternative System to Allocate Losses (COASTAL Act) Project within National Oceanic and Atmospheric Administration (NOAA). The authors acknowledge Dr. Andrew Kennedy for providing the in-situ wave data, Dr. Stylianos Flampouris for helping with Satellite Altimeter analysis and Drs. Zaizhong Ma and Avichal Mehra for providing the HWRF wind product and Dr. Andrew Cox for providing the OWI wind product. The author wish to thank Drs. Deanna Spindler and Roberto Padilla for fruitful discussions.

Appendix A. Supplementary data

Supplementary data to this article can be found online at https://doi.org/10.1016/j.coastaleng.2020.103656.

Appendix A. Statistical Analysis Summary

Table A.1
Models' performance at buoy locations summarizing linear regression and normal distribution statistical analysis in term of wind speed (m/s) and significant wave height (m) shown in Figs. 6 and 13. *All model configurations and results are pre-decisional and for official use only.*

#	Model	Var.	Forcing	Grid	Scheme	Par.	Δt [t]	Min	Max	$\bar{e}$	σ	|e|	RMSE	RB	Skill (NS)	Skill (OS)	Skill (T)
1	OWI	U_{10}	–	–	–	–	–	−15.87	8.95	−0.59	0.94	0.72	1.11	−0.08	–	–	1.07
2	WW3	H_s	OWI	Regular	Explicit	CD	(10,10,10,10)	−2.31	3.77	0.28	0.60	0.40	0.67	0.15	0.68	0.86	0.82
3	WW3	H_s	OWI	EC2001	Explicit	CD	(150,100,50,10)	−2.99	3.47	0.20	0.56	0.36	0.60	0.10	0.73	0.92	0.87
4	WW3	H_s	OWI	HSSOFS	Explicit	CD	(150,100,50,10)	−3.00	3.44	0.18	0.56	0.35	0.59	0.10	0.75	0.92	0.88
5	WW3	H_s	OWI	HSSOFS	Explicit	DD	(150,100,50,10)	−3.00	3.44	0.18	0.56	0.35	0.59	0.10	0.75	0.92	0.88
6	WW3	H_s	OWI	HSSOFS	Implicit	DD	60	−2.98	3.45	0.19	0.56	0.35	0.59	0.10	0.75	0.91	0.88
7	WW3	H_s	OWI	HSSOFS	Implicit	DD	600	−3.05	3.40	0.20	0.57	0.36	0.60	0.10	0.72	0.92	0.87
8	WW3	H_s	OWI	HSSOFS	Implicit	DD	1200	−5.02	3.66	0.22	0.62	0.37	0.62	0.11	0.7	0.93	0.85
9	HWRF	U_{10}	–	–	–	–	–	−17.49	4.64	−0.70	1.84	1.26	1.96	−0.10	–	–	1.11
10	WW3	H_s	HWRF	Regular	Explicit	CD	(10,10,10,10)	−3.22	3.62	0.19	0.59	0.37	0.62	0.10	0.75	0.93	0.89
11	WW3	H_s	HWRF	EC2001	Explicit	CD	(150,100,50,10)	−5.06	3.28	0.08	0.62	0.36	0.63	0.04	0.80	1.02	0.97
12	WW3	H_s	HWRF	HSSOFS	Explicit	CD	(150,100,50,10)	−5.02	3.26	0.06	0.62	0.36	0.62	0.03	0.82	1.02	0.97
13	WW3	H_s	HWRF	HSSOFS	Explicit	DD	(150,100,50,10)	−5.02	3.26	0.06	0.62	0.36	0.62	0.03	0.82	1.02	0.97
14	WW3	H_s	HWRF	HSSOFS	Implicit	DD	60	−4.99	3.15	0.07	0.61	0.36	0.61	0.03	0.82	1.01	0.97
15	WW3	H_s	HWRF	HSSOFS	Implicit	DD	600	−5.22	2.93	0.08	0.61	0.36	0.61	0.04	0.79	1.02	0.97

Table A.2
Models' performance at satellite altimeter tracks summarizing linear regression and normal distribution statistical analysis in term of wind speed (m/s) and significant wave height (m) *All model configurations and results are pre-decisional and for official use only.*

#	Model	Var.	Forcing	Grid	Scheme	Par.	Δt [s]	Min	Max	$\bar{e}$	σ	|e|	RMSE	RB	Skill
1	OWI	U_{10}	–	–	–	–	–	−11.29	14.08	0.23	1.77	1.26	1.78	0.03	0.95
2	WW3	H_s	OWI	Regular	Explicit	CD	(10,10,10,10)	−1.65	2.71	0.45	0.55	0.51	0.71	0.26	0.77
3	WW3	H_s	OWI	EC2001	Explicit	CD	(150,100,50,10)	−2.32	2.44	0.21	0.41	0.33	0.46	0.12	0.90
4	WW3	H_s	OWI	HSSOFS	Explicit	CD	(150,100,50,10)	−2.29	2.10	0.24	0.41	0.35	0.47	0.14	0.88
5	WW3	H_s	OWI	HSSOFS	Explicit	DD	(150,100,50,10)	−2.29	2.10	0.24	0.41	0.35	0.47	0.14	0.88
6	WW3	H_s	OWI	HSSOFS	Implicit	DD	60	−2.28	2.11	0.24	0.41	0.35	0.47	0.14	0.88
7	WW3	H_s	OWI	HSSOFS	Implicit	DD	600	−2.38	2.15	0.24	0.41	0.35	0.48	0.14	0.88
8	WW3	H_s	OWI	HSSOFS	Implicit	DD	1200	−2.38	2.15	0.25	0.42	0.36	0.49	0.14	0.88
9	HWRF	U_{10}	–	–	–	–	–	−11.20	11.07	0.05	1.39	0.98	1.39	0.01	0.98
10	WW3	H_s	HWRF	Regular	Explicit	CD	(10,10,10,10)	−2.73	2.16	0.35	0.44	0.41	0.57	0.20	0.83
11	WW3	H_s	HWRF	EC2001	Explicit	CD	(150,100,50,10)	3.66	2.51	0.18	0.42	0.30	0.46	0.10	0.93
12	WW3	H_s	HWRF	HSSOFS	Explicit	CD	(150,100,50,10)	−3.64	2.06	0.18	0.39	0.30	0.43	0.10	0.93
13	WW3	H_s	HWRF	HSSOFS	Explicit	DD	(150,100,50,10)	−3.64	2.06	0.18	0.40	0.30	0.43	0.10	0.93
14	WW3	H_s	HWRF	HSSOFS	Implicit	DD	60	−2.28	2.11	0.24	0.41	0.35	0.47	0.14	0.88
15	WW3	H_s	HWRF	HSSOFS	Implicit	DD	600	−3.22	2.08	0.19	0.39	0.31	0.44	0.11	0.92

Table A.3
Wave model performance at buoy observatories in term of significant wave height (m), shown in Fig. 10(a). *All model configurations and results are pre-decisional and for official use only.*

#	Model	Variable	Forcing	Grid	Scheme	Parallelization	Δt [s]	RMSD	σ	CC
1	Obs.	H_s	–	–	–	–	–	–	1.69	–
2	WW3	H_s	OWI	Regular	Explicit	CD	(10,10,10,10)	0.60	1.39	0.94
3	WW3	H_s	OWI	EC2001	Explicit	CD	(150,100,50,10)	0.56	1.52	0.94
4	WW3	H_s	OWI	HSSOFS	Explicit	CD	(150,100,50,10)	0.56	1.52	0.94
5	WW3	H_s	OWI	HSSOFS	Explicit	DD	(150,100,50,10)	0.56	1.52	0.94
6	WW3	H_s	OWI	HSSOFS	Implicit	DD	60	0.56	1.51	0.94
7	WW3	H_s	OWI	HSSOFS	Implicit	DD	600	0.57	1.51	0.94
8	WW3	H_s	OWI	HSSOFS	Implicit	DD	1200	0.62	1.76	0.94
9	WW3	H_s	HWRF	HSSOFS	Explicit	CD	(150,100,50,10)	0.55	1.97	0.96

Table A.4
Wave model performance at Satellite Altimeter tracks in term of significant wave height (m), shown in Fig. 10(b). *All model configurations and results are pre-decisional and for official use only.*

#	Model	Variable	Forcing	Grid	Scheme	Parallelization	Δt [s]	RMSD	σ	CC
1	Obs.	H_s	–	–	–	–	–	–	1.56	–
2	WW3	H_s	OWI	Regular	Explicit	CD	(10,10,10,10)	0.49	1.62	0.95
3	WW3	H_s	OWI	EC2001	Explicit	CD	(150,100,50,10)	0.33	1.66	0.98
4	WW3	H_s	OWI	HSSOFS	Explicit	CD	(150,100,50,10)	0.35	1.62	0.98
5	WW3	H_s	OWI	HSSOFS	Explicit	DD	(150,100,50,10)	0.35	1.62	0.98
6	WW3	H_s	OWI	HSSOFS	Implicit	DD	60	0.35	1.62	0.98
7	WW3	H_s	OWI	HSSOFS	Implicit	DD	600	0.35	1.62	0.98
8	WW3	H_s	OWI	HSSOFS	Implicit	DD	1200	0.35	1.63	0.98
9	WW3	H_s	HWRF	HSSOFS	Explicit	CD	(150,100,50,10)	0.32	1.63	0.98

Appendix B. Metrics for the evaluation of data-model agreement

The performance of atmospheric and wave models are assessed in terms of mean error ($\overline{e}$), absolute error $|e|$ relative Bias (RB), Root Mean Square Error (RMSE), standard deviation (σ), Pearson correlation coefficient (CC) and skill.

The mean error ($\overline{e}$) and absolute error $|e|$ show the systematic deviation from the observations and is given by

$$\overline{e} = \frac{1}{N}\sum_{i=1}^{N}(M_i - O_i) \tag{B.1}$$

$$|e| = \frac{1}{N}\sum_{i=1}^{N}|M_i - O_i| \tag{B.2}$$

where M_i is the modeled data, O_i is the measured data and N is the total number of observations.

The standard deviation is the square root of the variance. For data set X, consisting of N scalar observations, the standard deviation is defined as

$$\sigma = \sqrt{\frac{1}{N-1}\sum_{i=1}^{N}(X - \overline{X})^2} \tag{B.3}$$

where $\overline{X}$ is the mean of variable X. Relative Bias (RB) shows relative systematic deviation from the observations and is given by

$$RB = \frac{\sum_{i=1}^{N}(M_i - O_i)}{N\overline{O}} \tag{B.4}$$

The RMSE is given by

$$RMSE = \sqrt{\frac{1}{N}\sum_{i=1}^{N}(M_i - O_i)^2} \tag{B.5}$$

The Pearson correlation coefficient of two data sets is a measure of their linear dependence and is calculated by

$$CC = \frac{1}{N-1}\sum_{i=1}^{N}\left(\frac{M_i - \overline{M}}{\sigma_M}\right)\left(\frac{O_i - \overline{O}}{\sigma_O}\right) \tag{B.6}$$

where $\overline{M}$ and σ_M are the mean and standard deviation of model data $\overline{O}$ and σ_O are the mean and standard deviation of observations, respectively. It has a value between 0 and 1, where 1 is total positive linear correlation, 0 is no linear correlation.

The model skill is defined as

$$skill = 1 - \frac{\sum_{i=1}^{N} (M_i - O_i)^2}{\sum_{i=1}^{N} (|M_i - \overline{O}| + |O_i - \overline{O}|)^2} \tag{B.7}$$

References

Abdalla, S., 2012. Ku-band radar altimeter surface wind speed algorithm. Mar. Geodes. 35, 276–298. https://doi.org/10.1080/01490419.2012.718676.

Ardhuin, F., Louis, M., Rascle, N., Forget, P., Roland, A., 2009. Observation and estimation of Lagrangian, Stokes, and eulerian currents induced by wind and waves at the sea surface. J. Phys. Oceanogr. 39, 2820–2838. https://doi.org/10.1175/2009JPO4169.1.

Ardhuin, F., O'reilly, W., Herbers, T., Jessen, P., 2003. Swell transformation across the continental shelf. Part I: attenuation and directional broadening. J. Phys. Oceanogr. 33, 1921–1939. https://doi.org/10.1175/1520-0485(2003)033<1921:STATCS>2.0.CO;2.

Ardhuin, F., Roland, A., 2012. Coastal wave reflection, directional spread, and seismoacoustic noise sources. J. Geophys. Res.: Oceans 117. https://doi.org/10.1029/2011JC007832.

Battjes, J.A., Janssen, J., 1978. Energy loss and set-up due to breaking of random waves. In: Coastal Engineering, vol. 1978, pp. 569–587. https://doi.org/10.1061/9780872621909.034.

Benoit, M., Marcos, F., Becq, F., 1997. Development of a third generation shallow-water wave model with unstructured spatial meshing. In: Coastal Engineering, vol. 1996, pp. 465–478.

Berg, R., 2009. Tropical Cyclone Report: Hurricane Ike (Al092008), 1-14 September 2008. National Hurricane, Center.

Brown, D.P., Beven, J.L., Franklin, J.L., Blake, E.S., 2010. Atlantic hurricane season of 2008. Mon. Weather Rev. 138, 1975–2001. https://doi.org/10.1175/2009MWR3174.1.

Cardone, V., Cox, A., 2009. Tropical cyclone wind field forcing for surge models: critical issues and sensitivities. Nat. Hazards 51, 29–47. https://doi.org/10.1007/s11069-009-9369-0.

Chassignet, E.P., Hurlburt, H.E., Smedstad, O.M., Halliwell, G.R., Hogan, P.J., Wallcraft, A.J., Baraille, R., Bleck, R., 2007. The HYCOM (HYbrid Coordinate Ocean Model) data assimilative system. J. Mar. Syst. 65, 60–83. https://doi.org/10.1016/j.jmarsys.2005.09.016.

Chen, C., Beardsley, R.C., Cowles, G., Qi, J., Lai, Z., Gao, G., Stuebe, D., Liu, H., Xu, Q., Xue, P., Ge, J., Hu, S., Ji, R., Tian, R., Huang, H., Wu, L., Lin, H., Sun, Y., Zhao, L., 2013. An Unstructured Grid, Finite-Volume Community Ocean Model FVCOM User Manual, p. 416. C.

Cox, A., Greenwood, J., Cardone, V., Swail, V., 1995. An interactive objective kinematic analysis system. In: Fourth International Workshop on Wave Hindcasting and Forecasting, pp. 109–118.

Dietrich, J.C., Tanaka, S., Westerink, J.J., Dawson, C.N., Luettich, R.A., Zijlema, M., Holthuijsen, L.H., Smith, J.M., Westerink, L.G., Westerink, H.J., 2012. Performance of the unstructured-mesh, swan+adcirc model in computing hurricane waves and surge. J. Sci. Comput. 52, 468–497. https://doi.org/10.1007/s10915-011-9555-6.

Ferziger, J.H., Perić, M., 2002. Computational Methods for Fluid Dynamics, vol. 3. Springer.

Gopalakrishnan, S., Liu, Q., Marchok, T., Sheinin, D., Surgi, N., Tuleya, R., Yablonsky, R., Zhang, X., 2010. Hurricane Weather Research and Forecasting (HWRF) Model Scientific Documentation. Development Testbed Center.

Hasselmann, S., Hasselmann, K., Allender, J., Barnett, T., 1985. Computations and parameterizations of the nonlinear energy transfer in a gravity-wave specturm. Part II: parameterizations of the nonlinear energy transfer for application in wave models. J. Phys. Oceanogr. 15, 1378–1391. https://doi.org/10.1175/1520-0485(1985)015<1378:CAPOTN>2.0.CO;2.

Hersbach, H., 2016. The ERA5 atmospheric reanalysis. In: AGU Fall Meeting Abstracts.

Hope, M.E., Westerink, J.J., Kennedy, A.B., Kerr, P.C., Dietrich, J.C., Dawson, C., Bender, C.J., Smith, J.M., Jensen, R.E., Zijlema, M., Holthuijsen, L.H., Luettich Jr., R. A., Powell, M.D., Cardone, V.J., Cox, A.T., Pourtaheri, H., Roberts, H.J., Atkinson, J. H., Tanaka, S., Westerink, H.J., Westerink, L.G., 2013. Hindcast and validation of Hurricane Ike (2008) waves, forerunner, and storm surge. J. Geophys. Res.: Oceans 118, 4424–4460. https://doi.org/10.1002/jgrc.20314.

Hsu, T.-W., Ou, S.-H., Liau, J.-M., 2005. Hindcasting nearshore wind waves using a fem code for swan. Coast Eng. 52, 177–195.

Karypis, G., 2011. METIS and ParMETIS. In: Encyclopedia of Parallel Computing. Springer, pp. 1117–1124. https://doi.org/10.1007/978-0-387-09766-4_500.

Karypis, G., Kumar, V., 1999. Parallel multilevel series k-way partitioning scheme for irregular graphs. SIAM Rev. 41, 278–300.

Kennedy, A.B., Gravois, U., Zachry, B., 2010a. Observations of landfalling wave spectra during Hurricane Ike. J. Waterw. Port, Coast. Ocean Eng. 137, 142–145. https://doi.org/10.1061/(ASCE)WW.1943-5460.0000081.

Kennedy, A.B., Gravois, U., Zachry, B., Luettich, R., Whipple, T., Weaver, R., Reynolds-Fleming, J., Chen, Q.J., Avissar, R., 2010b. Rapidly installed temporary gauging for hurricane waves and surge, and application to hurricane gustav. Continent. Shelf Res. 30, 1743–1752.

Kennedy, A.B., Gravois, U., Zachry, B.C., Westerink, J.J., Hope, M.E., Dietrich, J.C., Powell, M.D., Cox, A.T., Luettich Jr., R.A., Dean, R.G., 2011. Origin of the hurricane Ike forerunner surge. Geophys. Res. Lett. 38 https://doi.org/10.1029/2011GL047090.

Li, J.-G., 2012. Propagation of ocean surface waves on a spherical multiple-cell grid. J. Comput. Phys. 231, 8262–8277.

Liau, J., 2001. *A Study of Wind Waves Hindcasting on the Coastal Waters*.. Ph.D. thesis PhD Thesis National Cheng Kung University, Tainan, Taiwan.

Luettich Jr., R.A., Westerink, J.J., Scheffner, N.W., 1992. ADCIRC: an Advanced Three-Dimensional Circulation Model for Shelves, Coasts, and Estuaries. Report 1. Theory and Methodology of ADCIRC-2DDI and ADCIRC-3DL. Technical Report. Coastal Engineering Research Center Vicksburg MS.

Mao, M., Van Der Westhuysen, A.J., Xia, M., Schwab, D.J., Chawla, A., 2016. Modeling wind waves from deep to shallow waters in lake Michigan using unstructured swan. J. Geophys. Res.: Oceans 121, 3836–3865.

Mao, M., Xia, M., 2017. Dynamics of wave–current–surge interactions in lake Michigan: a model comparison. Ocean Model. 110, 1–20.

Moghimi, S., Vinogradov, S., Myers, E.P., Funakoshi, Y., Van der Westhuysen, A.J., Abdolali, A., Ma, Z., Liu, F., 2019. Development of a Flexible Coupling Interface for Adcirc Model for Coastal Inundation Studies, vol. 41. NOAA technical memorandum NOS CS. https://doi.org/10.25923/akzc-kc14.

Patankar, S.V., 1980. Numerical Heat Transfer and Fluid Flow. hemisphere publ. *Corp.*, New York, p. 58.

Queffeulou, P., 2004. Long-term validation of wave height measurements from altimeters. Mar. Geodes. 27, 495–510. https://doi.org/10.1080/01490410490883478.

Queffeulou, P., Croiz é Fillon, D., 2012. Global Altimeter SWH Data Set-April 2012. Spatial Anography Laboratory, IFREMER.

Riverside Technology, Aecom, 2015. Mesh Development, Tidal Validation, and Hindcast Skill Assessment of an ADCIRC Model for the Hurricane Storm Surge Operational Forecast System on the US Gulf-Atlantic Coast. Technical Report.

Roland, A., 2009. Development of WWM II: Spectral Wave Modelling on Unstructured Meshes. Technische Universität Darmstadt, Institute of Hydraulic and Water Resources Engineering, Darmstadt. University.

Roland, A., Ardhuin, F., 2014. On the developments of spectral wave models: numerics and parameterizations for the coastal ocean. Ocean Dynam. 64, 833–846. https://doi.org/10.1007/s10236-014-0711-z.

Roland, A., Mewis, P., Zanke, U., Ou, S., Hsu, T., Liau, J., 2005. Verification and improvement of a spectral finite element wave model, waves 2005, ASCE/COPRI. In: Edge, Billy (Ed.), The Fifth International Symposium on Wave Measurement and Analysis. Madrid, Spain.

Roland, A., Zanke, U., Hsu, T.-W., Ou, S.-H., Liau, J.-M., 2006. Spectral wave modelling on unstructured grids with the WWM (wind wave model) I: the deep water case. In: Third Chinese–German Joint Symposium on Coastal and Ocean Engineering, Tainan, Taiwan, p. 17.

Roland, A., Zanke, U., Hsu, T.-W., Ou, S.-H., Liau, J.-M., Wang, S.-K., 2008. Verification of a 3rd generation FEM spectral wave model for shallow and deep water applications. In: 25th International Conference on Offshore Mechanics and Arctic Engineering. American Society of Mechanical Engineers Digital Collection, pp. 487–499.

Roland, A., Zhang, Y.J., Wang, H.V., Meng, Y., Teng, Y.-C., Maderich, V., Brovchenko, I., Dutour-Sikiric, M., Zanke, U., 2012. A fully coupled 3D wave-current interaction model on unstructured grids. J. Geophys. Res.: Oceans 117. https://doi.org/10.1029/2012JC007952.

Saha, S., Moorthi, S., Pan, H.-L., Wu, X., Wang, J., Nadiga, S., Tripp, P., Kistler, R., Woollen, J., Behringer, D., et al., 2010. The NCEP climate forecast system reanalysis. Bull. Am. Meteorol. Soc. 91, 1015–1058. https://doi.org/10.1175/2010BAMS3001.1.

Sørensen, O.R., Kofoed-Hansen, H., Rugbjerg, M., Sørensen, L.S., 2005. A third-generation spectral wave model using an unstructured finite volume technique. In: Coastal Engineering *2004*, vol. 4. World Scientific, pp. 894–906.

Theurich, G., DeLuca, C., Campbell, T., Liu, F., Saint, K., Vertenstein, M., Chen, J., Oehmke, R., Doyle, J., Whitcomb, T., Wallcraft, A., Iredell, M., Black, T., Da Silva, A. M., Clune, T., Ferraro, R., Li, P., Kelley, M., Aleinov, I., Balaji, V., Zadeh, N., Jacob, R., Kirtman, B., Giraldo, F., McCarren, D., Sandgathe, S., Peckham, S., Dunlap, R., 2016. The earth system prediction suite: toward a coordinated u.s. modeling capability. Bull. Am. Meteorol. Soc. 97, 1229–1247. https://doi.org/10.1175/BAMS-D-14-00164.1.

Tolman, H.L., 2002. Distributed-memory concepts in the wave model WAVEWATCH III. Parallel Comput. 28, 35–52. https://doi.org/10.1016/S0167-8191(01)00130-2.

Tolman, H.L., 2008. A mosaic approach to wind wave modeling. Ocean Model. 25, 35–47. https://doi.org/10.1016/j.ocemod.2008.06.005.

WW3DG, 2019. User Manual and System Documentation of WAVEWATCH III Version 6.07, the WAVEWATCH III Development Group. Tech. Note 316. NOAA/NWS/NCEP/MMAB url: https://github.com/NOAA-EMC/WW3/wiki/files/manual.pdf. link.

Zanke, U., Roland, A., Hsu, T.-W., Ou, S.-H., Liau, J.-M., 2006. Spectral wave modelling on unstructured grids with the wwm (wind wave model) II: the shallow water case. In: Third Chinese–German Joint Symposium on Coastal and Ocean Engineering (JOINT2006), Tainan, Taiwan.

Zhang, F., Weng, Y., Sippel, J.A., Meng, Z., Bishop, C.H., 2009. Cloud-resolving hurricane initialization and prediction through assimilation of Doppler radar observations with an ensemble Kalman filter. Mon. Weather Rev. 137, 2105–2125. https://doi.org/10.1175/2009MWR2645.1.

Zhang, X., Gopalakrishnan, S.G., Trahan, S., Quirino, T.S., Liu, Q., Zhang, Z., Alaka, G., Tallapragada, V., 2016. Representing multiple scales in the hurricane weather research and forecasting modeling system: design of multiple sets of movable multilevel nesting and the basin-scale HWRF forecast application. Weather Forecast. 31, 2019–2034. https://doi.org/10.1175/WAF-D-16-0087.1.

Zijlema, M., 2009. Parallel, unstructured mesh implementation for SWAN. In: Coastal Engineering *2008: (In* 5 Volumes*)*. World Scientific, pp. 470–482.

Zijlema, M., 2010. Computation of wind-wave spectra in coastal waters with SWAN on unstructured grids. Coast Eng. 57, 267–277. https://doi.org/10.1016/j.coastaleng.2009.10.011.